Mitigating the Coriolis Effect in Human Centrifuges by coherent G-misalignment

Mkhoyan, Tigran; Wentink, Mark; van Paassen, Rene; Mulder, Max; de Graaf, B

DOI
10.2514/6.2019-0714

Publication date
2019

Document Version
Final published version

Published in
AIAA Scitech 2019 Forum

AIAA SciTech Forum
7-11 January 2019, San Diego, California
AIAA Scitech 2019 Forum

10.2514/6.2019-0714

Mitigating the Coriolis Effect in Human Centrifuges by Coherent G-misalignment

T. Mkhoyan,*M. Wentink,†M. M. van Paassen,‡M. Mulder,§and B. de Graaf¶
Delft University of Technology, Delft, The Netherlands
and
Desdemona BV, Soesterberg, The Netherlands

When coupled with additional degrees of freedom, centrifuge-based motion platforms can combine the agility of an hexapod-based motion platform with the ability of sustaining higher G-levels and an extended motion space. This combination of motion characteristics is required for realistic simulation of extreme flight scenarios. However, a false and often nauseating sensation of rotation, the so-called Coriolis effect, induced by the central yaw rotation, combined with the simultaneous rotation of the centrifuge cabin (passive Coriolis effect), or pilot's head (active Coriolis effect), is the main disadvantage of any centrifuge-based motion platform. For this reason, the majority of human centrifuges are used solely as passive G-trainers in relatively short sessions. This paper discusses the development of a novel motion filter which aims to minimize the undesired Coriolis effects, by allowing for small mismatches in the alignment of pitch or roll coordination. Numerical studies showed that this Coherent Alignment Method (COHAM), is capable of reducing the angular accelerations, while constrained to operate within a region of coherent alignment, the Coherent Alignment Zone. In order obtain data to construct the CAZ region, i.e., establish body tilt thresholds in pitch and roll, an experiment was carried out in the Desdemona motion simulator. Results show higher thresholds in pitch and also higher ambiguity in pitch perception. A follow-up study is planned to further develop and experimentally validate our novel, predictive motion filter, based on the established CAZ region.

Nomenclature

Ω_ψ	= centrifuge yaw velocity	G_z	= inertial body vector, positive downward
G_y	= inertial body vector, positive sideways right	G_x	= inertial body vector, positive backward
N_z	= normal acceleration	t	= time
${}^h\alpha_x$	= head-x angular acceleration	${}^h\alpha_y$	= head-y angular acceleration
${}^h\alpha_z$	= head-z angular y-acceleration	Ω_{psi}	= centrifuge central yaw rate
a_R	= linear radial acceleration	a_t	= linear tangential acceleration
$\theta_{true}(t)$	= true cabin angle response	$\theta_{COHAM}(t)$	= cabin angle response with mismatch
n_{SCC}	= neuronal discharge rate	γ	= input angular acceleration
H_{SCC}	= Hosman et al. tranfer function	R_γ	= perceptual angular acceleration

I. Introduction

Until recently, the application of centrifuges (see Figure 1) in pilot training was mainly restricted to passive G-training in which the pilot has no control over the Degrees-of-Freedom (DOF). The applicability of passive G-training is

*Ph.D. student, Faculty of Aerospace Engineering, Aerospace Structures and Materials and Control & Simulation department, T.Mkhoyan@tudelft.nl, P.O. Box 5058, 2600GB Delft, The Netherlands.
†Director technology, Desdemona B. V. mark.wentink@desdemona.eu, Kampweg 5, 3769 DE Soesterberg, The Netherlands.
‡Associate Professor, Faculty of Aerospace Engineering, Control and Operations department, M.M.vanPaassen@tudelft.nl, P.O. Box 5058, 2600GB Delft, The Netherlands
§Professor, Faculty of Aerospace Engi1neering, Control and Operations department, M.Mulder@tudelft.nl, P.O. Box 5058, 2600GB Delft, The Netherlands, AIAA Associate Fellow.
¶Director, Desdemona B. V. , bernd.degraaf@desdemona.eu, Kampweg 5, 3769 DE Soesterberg, The Netherlands.

limited to testing the pilot's capability of sustaining a certain G-plateau (up to 9G) for a specific period of time (10 seconds) without losing consciousness (known as G-force induced loss of consciousness (G-LOCK) [1]). In contrast, in active G-training, the pilot has control over one or more DOF which allows simulation of realistic fighter scenarios.

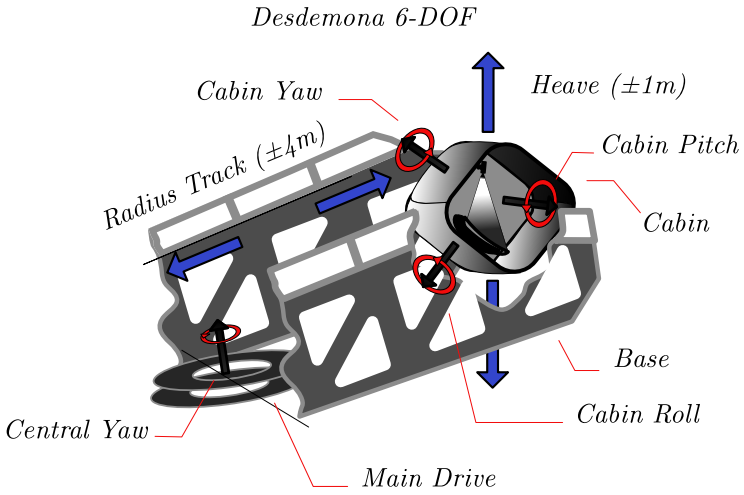

Figure 1 Desdemona 6-Dof Simulator axis convention.

Sustaining elevated G-levels, while carrying out a mentally demanding task, is one of the most challenging aspects of fighter aircraft piloting. The strain induced by high G-levels has been known to deteriorate pilot's tracking performance and decision-making [2]. Real-life fighter pilot training is associated with high costs and considerable safety risks for pilots. Active G-training has the potential to provide a realistic platform where pilots can safely practice dangerous scenarios at much lower cost.

However, the main issue related to the application of human centrifuges is the so-called vestibular Coriolis cross-coupling (or Coriolis rotations) induced at the position of the pilot's head, during simultaneous rotations of the cabin and the centrifuge's central yaw rotation. When referring to Coriolis rotations, a distinction is made between passive and active Coriolis. In *passive* Coriolis, the pilot head is fixed and the cross-coupling is caused by the cabin motion required to align the G-vector, through maintaining a particular cabin orientation. In *active active* Coriolis, the cross-coupling is caused by pilot-controlled, active self-rotations of the head in free space. While active Coriolis cannot be controlled, passive Coriolis, can, which is the subject of this paper.

In most practical flight scenarios (e.g., pulling sharp turns in an F-16) the subject must be aligned with the resultant G-vector along the vertical axis, as illustrated in Fig. 2b. The figure shows a typical case of cabin alignment under a constant 2G-level rotation (centrifuge yaw rate of 2.06 rad/s), where the cabin vertical axis (yaw) is aligned (in this case in 60 deg pitch) with the subject's G_z-axis, as depicted in Fig. 2a. The magnitude of the G-level is dictated by the amount of angular rotation of the centrifuge's central yaw-axis. For each change in G-level, a transient referred to as G-onset, the cabin must rotate accordingly to maintain a correct alignment of the resulting G-vector. This combination of cabin alignment rotation and the centrifuge's yaw rotation induces a passive Coriolis effect. Both the central yaw and the cabin alignment rotations are proportional to the magnitude of the experienced Coriolis rotation: the higher the rotation, the stronger the effect. Hence, to mitigate the passive Coriolis effect, either one or both rotations would need to be made smaller. Since the central yaw rotation must be maintained to realistically simulate the required G-level, the cabin alignment rotation *could* perhaps be made smaller, *if* a certain deviation is allowed from the correct alignment, for instance in case pilots cannot perceive these small alignment deviations.

In [3], the concept of minimizing the cabin alignment rotation in an attempt to reduce undesired Coriolis rotation, was developed and tested. This led to the development of a novel motion filter, based on the so-called Coherent Alignment Method (COHAM). The principle of the COHAM is to align the simulator cabin with minimal amount of cabin rotation, while not allowing the pilot to notice the mismatch in the G_z-alignment during each G-onset. The positive (upward) and negative (downward) limits of the mismatch are determined by the hypothetical Coherent Alignment Zone (CAZ) region, defined as a region where the deviation from the correct cabin angle, θ_{true}, is still perceived as coherent

and consistent. To this end the concepts of a novel motion filter based on COHAM, were developed in this paper, and an experiment was performed to establish a coherence zone, CAZ, for cabin angle mismatch in the presence of elevated gravitational condition.

This paper is structured as follows. First a brief overview is given on the basics of centrifuge cueing. Then the concept of the coherence zone, CAZ, and cabin alignment mismatch using COHAM is explained. This is followed by simulation studies using a 1.4 G onset and simplified 3-channel perception model to study the perceived coriolis rotations. The remainder of the paper describes the experiment that was set-up in order to obtain threshold values for the CAZ region for the further development of the COHAM motion filter.

II. Centrifuge cueing

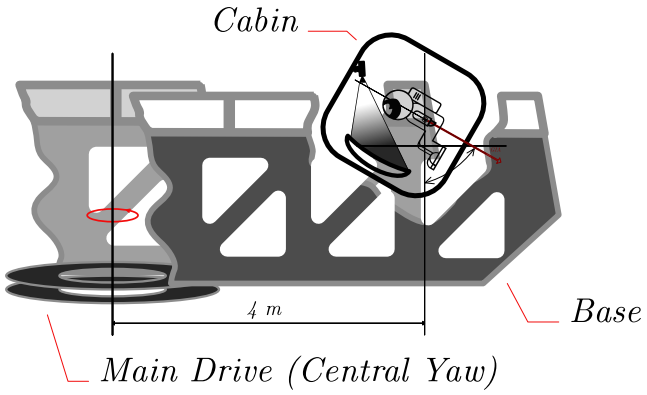

(a) Schematic overview of the subject's relative orientation in the Desdemona simulator, configured for the 'Rocket Man' cueing (i.e. alignment using pitch rotations).

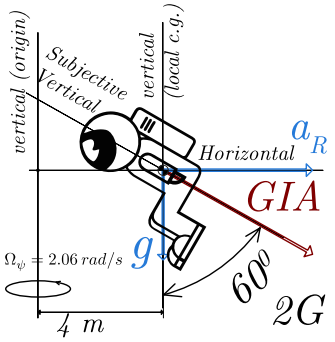

(b) Free Body Diagram of linear accelerations at constant centrifuge yaw rotation of 2.06 rad/s.

Figure 2 Schematics of subject's orientation in centrifuge cueing in the Desdemona simulator.

In order to attain sustained G-levels, the centrifuge base needs to spin along the central yaw axis. This yaw velocity, denoted as, Ω_ψ can be as high as 150 degrees/s [4] in the Desdemona. The desired constant G-level, usually referred to as the magnitude of the resultant Gravito Inertial Acceleration (GIA) or, Gravito Inertial Force (GIF), corresponds to a steady-state $\Omega_{\psi_{ss}}$ value (see Figure 3). From the perspective of the pilot situated in the cabin, the GIA coincides with the gravitational acceleration z-direction G_z for most practical simulation scenarios. A free body diagram of forces is shown in Figure 2b for the case of constant centrifugation at 2G level.

The resultant G-vector, also referred to as GIA, can be expressed as follows:

$$GIA = \sqrt{{a_t}^2 + {a_R}^2 + g^2} \tag{1}$$

Here a_t and a_R are the tangential and radial linear accelerations resulting from centrifugation, and g the gravitational constant. a_R can be expressed as:

$$a_R = \frac{v^2}{r} = (\Omega_\psi)^2 \cdot R \tag{2}$$

A typical relationship between the centrifuge yaw-rate and G-level is shown in Fig. 3. This figure represents the steady state G-level of the Desdemona simulator, with a radius track of four meters shown in the schematics of Fig. 2. During the centrifugation phase, the cabin, or the gondola in case of a conventional centrifuge, needs to swing out to keep the true orientation of the human-vertical axis G_z with respect to the resultant G-vector. The steady-state cabin angle required for alignment ($\theta_{true}\,(t)$) can be found from the following relation:

$$\theta_{true}\,(t) = \arctan\left(\frac{a_R}{g}\right) = \arctan\left(\frac{(\Omega_\psi)^2 R}{g}\right) \tag{3}$$

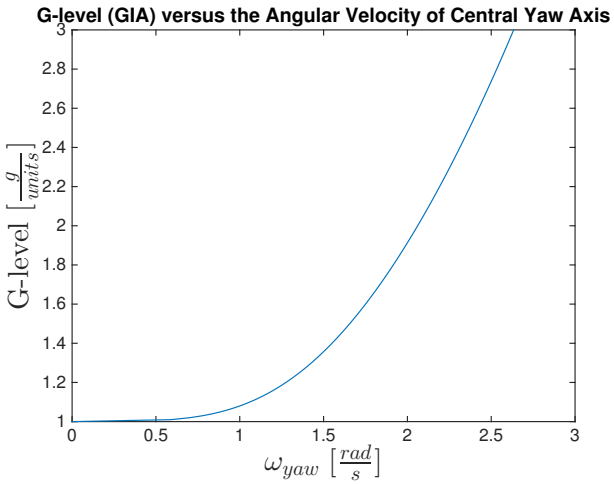

Figure 3 Resultant G-vector (GIA) versus the steady state yaw-rate of the Desdemona's central yaw-axis, $\Omega_{\psi_{ss}}$

The quadratic relationship suggests, that the higher G-levels require increasingly higher yaw-rates. This is turn requires an appropriate cabin rotation. The relationship between the alignment angle and the GIA similarly has a quadratic relationship as shown as the blue (true) curve in Figure 3.

When the cabin is allowed to have a DOF of angular rotation (roll or pitch), in an axis other than that of the main yaw-axis, simultaneous rotations will induce a Coriolis effect [5]. For the pilot situated inside the cabin, this cross-coupling can be experienced as a sensation of tumbling, nausea and or dizziness [6]. This is an inevitably negative and a highly undesired effect of all centrifuge-based simulators.

Although the Coriolis effect is related to the vestibular responses of the Semi Circular Canals (SCC) and is given form by the subject's non-exact perception, the kinematic source behind the Coriolis effect has an exact form. Considering that the pitch, roll and yaw SCC canals have a specific orientation* with respect to the horizontal plane, the angular acceleration arriving at the pilots head can be decomposed into three axes as shown in Figure 4[7]. The resulting angular accelerations are the head-centric, ${}^h\alpha_X$, ${}^h\alpha_Y$ and ${}^h\alpha_Z$, accelerations by Holly [7–9]:

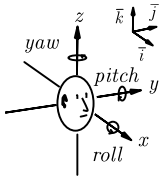

$$ {}^h\boldsymbol{\alpha} = \begin{bmatrix} {}^h\alpha_X \\ {}^h\alpha_Y \\ {}^h\alpha_Z \end{bmatrix} = \begin{bmatrix} \ddot{\theta} \\ \Omega\dot{\theta}\cos(\theta) + \dot{\Omega}\sin(\theta) \\ -\Omega\dot{\theta}\sin(\theta) + \dot{\Omega}\cos(\theta) \end{bmatrix} \tag{4} $$

Figure 4 Standard coordinates and unit vectors for specification of head Angular Motion (from [7]).

This set of equations describe a typical case of head tilt, rotation around head-centric-axis, in the presence of simultaneous whole body rotation. The latter represents the default, 'Rotating chair', configuration for fundamental Coriolis related experiments [9, 10]. Here, θ represents the angular displacement around head-x-axis, the $\dot{\theta}$ the angular velocity, $\ddot{\theta}$ angular acceleration, Ω, the velocity of the rotating reference frame and, $\dot{\Omega}$,the acceleration of the rotating frame. This example can be superimposed to centrifuge roll alignment under constant yaw rotation of the base, while a subject is situated inside the centrifuge cabin. As shown above, the initiated rotation in x-axis causes a coupling in two other axes, the magnitude of which depends both on the product of the initiated rotation (in the form of angular displacement and angular rate) and the centrifuge yaw rotation (in the form of angular velocity and angular acceleration). Reflecting back to the previous reasoning, Ω was the parameter that could not be controlled (determines realistic G's), while θ could be controlled under the assumptions of COHAM. In particular, reducing the latter, would directly reduce the magnitude of the kinematic source of coupled angular accelerations and thus the perceived Coriolis rotations at the respective SCC canals.

*The exact orientation differs from person to person. Yaw-axis is, in fact, sightly tilted downward in order to accommodate our default orientation of the head (slightly looking downward)

A. Background of the study

Desdemona BV. [11], has developed and implemented two G-cueing solutions over the years. The first, is a conventional solution where the pilot in the simulator faces the direction of rotation and is aligned with the resultant gravito-inertial vector G_z using the roll-axis. The second, is a solution where the pilot faces inward towards the centre of rotation and is aligned using the pitch axis in Figs. 2b and 2a. This G-cueing solution, nicknamed the "Rocket Man", is shown in 2a. Based on experiences from practical trainings and some limited experiments, the latter solution was found to be more comfortable and appears to cause less motion sickness. Although, no scientific basis exists to support the statement, the coordination in pitch with the 'pilot facing inward'- solution was preferred and resulted in a less (noticeable) Coriolis effect. In this study the advantages of aligning in either pitch (Rocket Man) or roll (conventional) were investigated in order to establish which of the two configurations served as a better basis for novel motion cueing approach. To this end and an experiment was performed in order to establish a coherence zone for cabin angle mismatch, called the CAZ in the presence of elevated gravitational condition. The suggested novel cueing method, called the COHAM, utilizes the boundaries of the hypothetical CAZ in order to coordinate the simulator cabin with the least amount of pitch motion possible without the pilot noticing the mismatch in the G_z-alignment.

III. Hypothesis

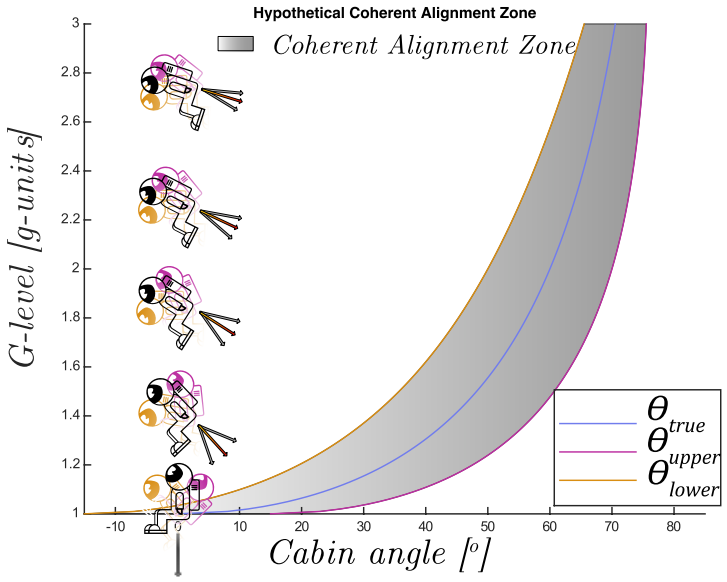

Figure 5 Hypothetical Coherent Alignment Zone [3]

A. Concept of Copherent Alignment Zone

Assuming for a moment that such a mismatch is allowed, a region can be defined, herewith referred to as the Coherent Alignment Zone (CAZ), where the deviation from the true alignment angle, herewith referred to as θ_{true}, is still perceived as coherent and consistent (illustrated in Fig. 5). The concept of coherence zone was defined in the earlier studies of Van Der Steen [12] and Pais [13]. These studies were interested to find the limits of the coherence zone, beyond which a coherence no longer exists between the visual and inertial stimuli and the subject is able to detect a mismatch. Van der Steen measured the inertial motion in terms of amplitude for yaw, roll, swing (sway and roll combined), surge and heave. He did so varying the visual motion amplitudes (0-12 deg/s for roll and sway, 3-18 deg/s for yaw and 0.5 m/s for linear) and frequencies (between 1-2 rad/s). CAZ shows analogy to this approach, however, the key difference is in the two measures that define the mismatch. In case of the CAZ it is the GIA-magnitude and the alignment angle, while in case of Van der Steen the measures were the visual motion and the inertial motion.

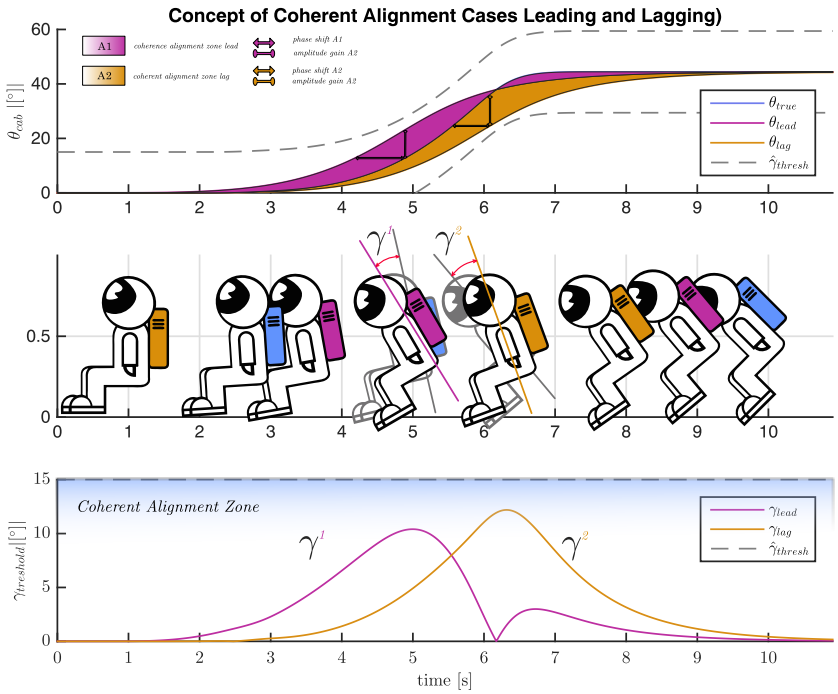

Figure 6 Illustration of the COHAM for a single cabin alignment in pitch from 1G to a baseline level of 1.4G [3]

B. Coherent Alignment Method

The concept of a coherence zone, and the idea that minimising the cabin alignment rotation could reduce the Coriolis effect, led to development of a motion filter, that utilizes *coherent alignment* of the cabin angle. The principle of the so-called Coherent Alignment Method (COHAM) is to align the simulator cabin with the least amount of motion possible, i.e., without the pilot noticing the mismatch in the G_z-alignment. The mismatch is introduced as a positive (upward) or a negative (downward) offset angle w.r.t. to the correct cabin angle required to align with the resultant G-vector for a given G-onset. The boundary inside which the COHAM operates is determined by the maximum allowable mismatch definition by the CAZ.

In a practical application for a motion filter that commands the cabin angle signal, two cases are possible, either lagging behind the true signal (lagging mechanism) or leading the true signal (leading mechanism). An illustration of the COHAM for a typical G-onset from 1G to a steady state level of 1.4 G is shown in Fig. 6. Here, the pilot icon represents the subject's orientation in the cabin for the cases of rotation with lag (yellow), lead (magenta) and true (blue). The leading mechanism starts pitching earlier than the true one, which is still in upright position at that moment. The lagging mechanism lags with respect to the true and towards the end it lags a bit less.

To test this method, the true cabin angle was filtered with the filter set-up as shown in Fig. 7b for the leading and lagging mechanisms. The signals were generated by a two step filtering where first a phase delay was added, after which the signal was filtered with a first order low-pass filter. The parameters of the time constants were calculated such that the resulting response did not exceed the hypothetical CAZ boundary indicated by an upper and lower threshold of 15 degrees (see Fig. 7b). Figure 7a shows the zoomed region of the cabin angle responses.

The lower subplots show how the angular velocity and the angular accelerations (middle and lower subplots) are significantly reduced by utilizing either the leading or lagging mechanism. Even more importantly, the onset of the angular acceleration peaks was shifted to a region with lower centrifuge yaw magnitude, further reducing the product of two angular rotations (shown in Eqs. 4) and, thus, less kinematic cross-coupling.

C. Analysis of COHAM with SCC Perception model

While the previous analysis confirms the reduction of physical angular velocities and thus the coupled physical coriolis accelerations, the question still remains how this filter is perceived by human vestibular system. To analyze this a simplified 3-channel perception model, Augmented Coriolis Response Model (ACRM), is proposed representing the SCC and the coupling of rotation in the three head-centric axes ${}^h\alpha_x$, ${}^h\alpha_y$ and ${}^h\alpha_z$. The perception model is based on the Hosman et al. SCC model [14], Holly's Kinematic model, and the coordinated system [8] shown in Fig. 4. For the ACRM model it was assumed that each SCC channel has the same dynamics represented by the Hosman et al. second-order filter model:

$$H_{SCC}(j\omega) = \frac{n_{SCC}}{R_{\ddot{y}}} = \frac{(1 + 0.11j\omega)}{(1 + 5.9j\omega)(1 + 0.005j\omega)} \tag{5}$$

More explanation regarding the transfer function is given in Appendix E. To study how the COHAM filter impacted this perception model, the COHAM filtered cabin alignment signal and the accompanying 1.4 G-onset of the central yaw axis of the previous example, were filtered with the ACRM filter. The result is shown in Figure 8b. As seen from the graphs, the ACRM response of the leading system (magenta curve) results in lowest magnitude of the head-centric filtered angular accelerations in all axes. In contrast, the lagging ACRM response (yellow curve) has a higher peak in head-Z axis. The higher magnitude in Z axis is due to shift of the cabin velocity peak towards the saturation limit of the transient angular yaw velocity response of the motion system. In other words, both the sinus term (due to higher θ displacement) as well as the product $\dot{\theta}_{lag}$ and Ω_{yaw}, have a greater negative impact in ${}^h\alpha_z$ and thus stronger effect. This results in larger negative peak of ${}^h\alpha_z$ (dashed grey curve) in Figure 8a. However, we must evaluate the magnitude of individual angular accelerations components in relation to responses from opposite axes. Doing so, the advantage of lagging system over the true response is clearly visible by a significant reduction (up to 2 $[^\circ/s^2]$) of head-X and head-Y with angular acceleration peaks.

It must be noted that the graphs do not show the full transient ACRM responses. When examining the timescale of the plots one sees that due to delay and dampening, the perceived acceleration 'sensation' prolongs after the mathematical angular acceleration have subsided.

By utilizing the COHAM it can thus be seen, that significant reduction is made in rotation velocity and acceleration with respect to the true angle. Both mechanisms sweep through the CAZ region, introducing a mismatch response, as shown in the lower subplot. However, since the threshold is not exceeded, the motion is, still believed to be coherent.

It must be noted, that the analysis shown in section III.B and III.C is done off-line, and so full knowledge of the signal existed. In order to practically apply this method to a motion filter, a predictive approach is required to correctly time the peak of the onset, such that the motion cue is true and achieves lowest rotational velocity. The crux of the timing and prediction is related to optimal use of the CAZ boundary and was tackled in the follow-up study. For the

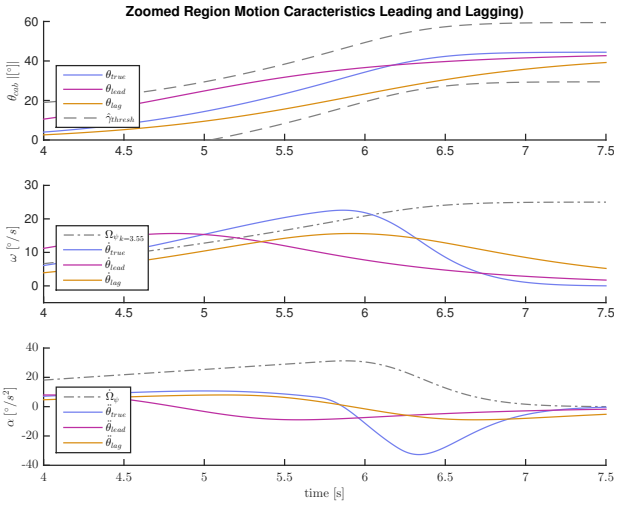

(a) Response characteristics of pitch motion with lead and lag. The curves describe lagging and leading cabin roll alignment by means of rotation in pitch.

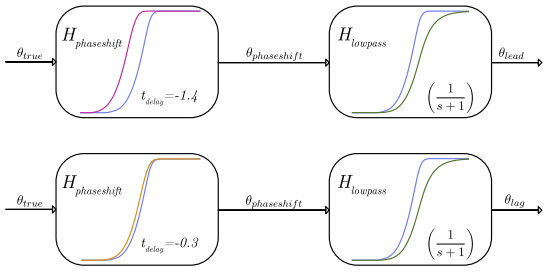

(b) Two step filtering of the true cabin roll signal (blue line) for leading and lagging mechanisms. The first step adds a phase delay to the signal and in the second step signal is further dampened and delayed. Note that negative t-delay corresponds to leading phase shift.

Figure 7 Leading and lagging mechanism simulations for 1.4 G onset.

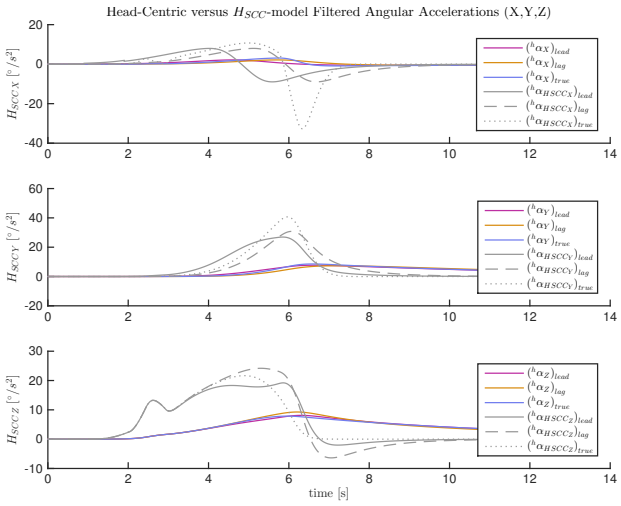

(a) Head-Centric (X,Y,Z) ACRM Filter Response and Head-Centric Angular Accelerations (X,Y,Z) Induced by Cabin (Roll) Rotation Around Head-X Axis.

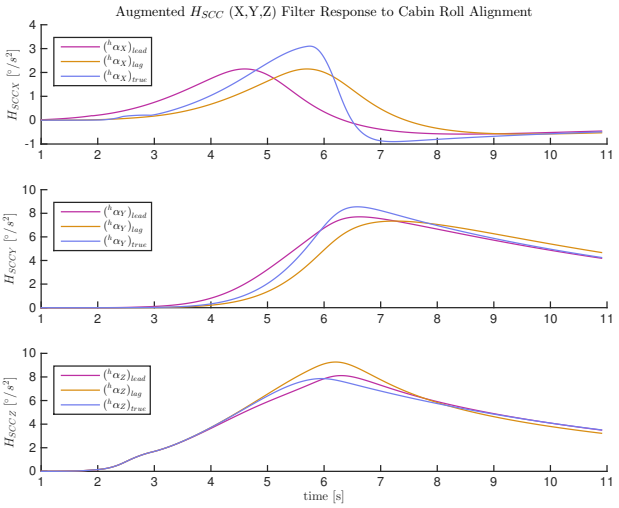

(b) Zoomed Region of Head-Centric (X,Y,Z) ACRM Filter Response to Cabin (Roll) Rotation Around Head-X Axis.

current study, this analysis was meant to merely investigate whether the method would provide a significant reduction of the angular rates ($\approx$ 7 deg/s) and accelerations ($\approx$ 7 deg/s^2). In addition, the hypothetical CAZ threshold of 15 degrees was used here, which still needed validation. This prepared the work for the next phase of the study, in which the CAZ zones were established by means of an experiment, as will be explained next section.

IV. Experiment

In order to establish body tilt perception thresholds under elevated G-levels (1 - 1.4G) in pitch and roll axes, an experiment was conducted in the Desdemona motion simulator facilitated by the Desdemona B.V.[11] based in Soesterberg, the Netherlands. The goal of the experiment was to investigate if the CAZ existed and how the gravitational conditions influenced the perception of CAZ.

A. Previous Research

There are many resources available regarding perception of body tilt, however, due to complexity and lack of apparatus capable of centrifugation with multiple degrees of freedom, resources regarding body tilt thresholds estimation under high gravitational loads in human centrifuges, are less abundant. The majority of the experiments are passive experiments with 2 degrees-of-freedom (central yaw spin and roll alignment of the gondola). Tribukait, one of the few currently active researchers in this area, made a significant effort to study the perception of roll tilt during gondola (cabin) centrifugation [15–18] in the Sweden's 4 degrees of freedom centrifuge (Dynamic Flight Simulator). The latter is, one of the few centrifuges with the ability to face the pilot forward, backward and sideways relative to the centrifugation direction [19].

Classical examples studying the perception of self-orientation relative to the gravity, make use of the Subjective Visual Vertical (SVV) Subjective Visual Vertical (SVV) or Subjective Visual Horizontal (SVH) Subjective Visual Horizontal (SVH) as their their tool of assessment. In these types of experiments, the subjects are asked to adjust a luminous line on a display, with their perceived earth-centric vertical or horizontal body orientation, the SVH or SVV [20–22].

Tribukait [17, 19] used this method, to investigate the sensation of roll tilt at different phases of centrifugation (loading and unloading of G-forces, G-plateaus). Here the SVV is measured by means of an adjustable luminous line in darkness under 1.1 G, 1.7 G, and 2.5 G levels. Another experiment also focused on investigating the role of otoliths in perception of roll-tilt [18] for several G-onset profiles. Although centrifuge related, these studies investigated the passive post-centrifuging effects rather than introducing and active tilt (alignment mismatch) to the subject.

In the 60's study, Stewart et al., intended to determine the supra-threshold for Coriolis acceleration in a human centrifuge [23], with active roll and pitch rotations at various gravitational levels (up to 1.8 G). The simulator used

for the experiment, located at Ames Research Center, was a 5 degrees of freedom centrifuge. However, unlike the Desdemona, it did not have the capability to travel the cabin along the linear radius track, and the arm was fixed at 30 feet. The results obtained therein, however, showed dependency to apparatus due to noise induced by the central yaw track while rotating. The disturbance was responsible for levels as high as 0.3 G vertical. Additionally, the flexible cabin hood was poorly isolated from the outside environment, hence vibrational and sound cues are likely to contribute to perception related studies.

Another set of experiments concentrated on identifying the self-tilt perception by means of oculomotor cues [24], the feedback of the brain from the eye muscles, an a comparison study by van Beuzekom et al., to investigate differences encountered in visual versus oculomotor stimulus [22]. Many studies, such as the one carried out by Beuzekom et al. put an emphasis in the role of otoliths regarding head or whole body-tilt when modeling human sensory estimators. An interesting example is a study conducted by Tarnutzer et al. investigation of the otolith-dependent variability of the SVV with regard to orientation of the GIF [25]. To be specific, the study was intended to point out a decrease in effectiveness of otolithic feedback, likely to produce higher variability in SVV, during roll-tilt perception that was suggested by the results from their otolith-estimator models. Their finding suggests that decreasing the effectiveness of the otolith-estimator with increasing roll was able better predict the SVV variability as suggested by their experimental findings. This phenomenon was previously explained by Schoene and de Haes as decreasing *effectiveness* of the otolith organs with increasing head tilts [26]. Although the introduced roll-tilt angles were much higher (up to 180°) in these studies, this is an interesting aspect to keep in mind when discussing the results from the current experiment.

Another method of measuring the subject's self-orientation estimate relative to the GIA is the nulling method used to study the latency of detection steps of linear acceleration steps [27] in the absence of visual cues. Herein, the subject has an active role of returning to the perceived upright, perfectly upright sitting position, after an initial displacement has been introduced. Threshold measurements from early studies found a success rate of 75 % when the subjects were tilted away from the vertical, given that the tilt exceeded 2.2° [28]. The latter corresponds to a lateral component of 0.038 G-units. This is interesting data to compare to the current experiment. However, the subject does not have an active role in the experiment and as suggested by Young [27] this may involve additional complexity in the estimator dynamics. Furthermore the conditions in the current experiment include elevated G-levels. This is believed to have a strong impact on the detection time, adding to the complexity of estimator dynamics.

1. Relevance

The main difficulties of extrapolating these result obtained in these studies to a practical G-cueing solution is that the experimental conditions almost never can be replicated in one-to-one fashion. In psychometric experiments with centrifuges, the apparatus, setup (ergonomics, chair etc) in combination with specific visuals and motion stimulus (vestibular input), are known to strongly affect subject's perception of body orientation. This is more so in the case that more elements of the human sensory system are involved. When a human subject is given the possibility to tap into the full capability of his/her sensory system, the perception process becomes very complex. This indicates the challenging aspect of psychometric experiments, namely, non-linearity of the human. The reflection on the literature can be closed by the notion that this experiment attempts to exclude the estimation-process influenced by the visual coupling, and focuses more on the somatosensory and static otolith cues. This has the potential of obtaining a more fundamental type of perception thresholds, possibly limiting the apparati dependency.

B. Hypotheses

Based on the background information given previously the research question posed in this experiment can be formulated as follows:

What are the differences in human perception thresholds of sideways (Roll) and forward-backward (Pitch) tilt angle and how does the gravitational environment affect this.

Hypotheses that were tested in this experiment were:

- Due to lack of opposite differential somatosensory interface along the body symmetry axis, the cabin pitch angles will be less apparent and will therefore result in higher perceived thresholds and spread.
- Higher gravitational resultant force will induce, both higher somatosensory differential as higher somatosensory absolute response, thereby decreasing the Roll and Pitch thresholds, respectively. Pitch thresholds are expected to be affected less due lack of the differential interface mechanism.
- Additionally, due to the increase in amplitude of the resultant gravitoinertial acceleration, the time to detect of the

of the linear acceleration steps is expected to drop, thereby increasing the accuracy of otolith-estimator at higher G-levels. This is expected to contribute to the overall reduction of the threshold levels.

C. Method

1. Experiment Design

The design of the experiment is composed of a three-way repeated measures within subjects design. In this experiment, 12 naive subjects (without piloting experience) were introduced to sub- threshold pitch and roll tilt motion (0.4 deg/s and maximum of 20 degrees) in random order and asked to perceive the direction of the tilt with respect to the perfectly upright sitting position. The motion conditions that were tested, were: 1G, 1G with central yaw rotation and no additional gravity, and 1.4 G in an elevated G-environment.

2. Apparatus

The experiment was conducted in the Desdemona motion simulator, depicted in Figure 9. This motion simulator was commissioned by TNO research institute and was manufactured by a shared effort from the manufacturer AMST located in Austria and the researchers at TNO. The key aspect that sets this motion simulator apart from both hexapod based simulators as centrifuges based simulators are the degrees of freedom in combination with sustained G-load capability.

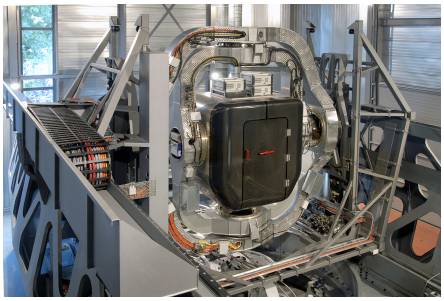

Figure 9 Desdemona Simulator located at Soesterberg, The Netherlands

While a conventional centrifuge has generally two degrees of freedom, Desdemona combines its sustained G-load capability with five degrees of freedom. Control of all six degrees of freedom are available in hexapod mode (no centrifugation). The simulator has a fully gimballed 3-DoF mounted cabin allowing 360 degrees of rotation. Furthermore the cabin as a whole can travel longitudinally along a linear arm of 8 meters and along the heave axis up to 2 meters. Lastly the entire structure can rotate around the central axis to generate the centrifugal motion up to a maximum of 3G when the horizontal axis is locked.

3. Experimental Variables

Control Variables The angular displacement of the cabin, in Pitch and Roll, were varied at a constant 0.4 degrees per second angular velocity, well below the approximated human rotation perception levels of critical rotational velocity of 2.5 degrees per second [27]. Furthermore the cockpit configuration of the cabin was kept constant for all of the subjects. The cockpit was fitted with a generic helicopter layout and a typical cyclic control that was used for the pilots input. The pilots were assigned a passive task of registering the perceived tilt by means of a 4 directional hat switch (cursor) on the cyclic. The experiment was carried without additional visuals, under dimmed lighting conditions. Figure 11 shows the cursor along with the convention used for button input.

Independent Variables The experiment was designed to study the effect of the gravitational conditions on the human perception of body tilt. Throughout the duration of the trial, the Pitch and Roll attitude of the cabin was varied between $\pm 20^{\circ}$ from the upright, while the gravitational condition was fixed for one of the three condition (C1, C2 or C3). Independent Variables thus were, the Axis (2 levels), Direction (2 levels) and G-Condition (3 levels). The respective levels are Roll and Pitch; + (Roll Right or Pitch Down) and - (Roll Left or Pitch Up); and 1G, 1Gyaw and 1.4G as shown in Table. 1.

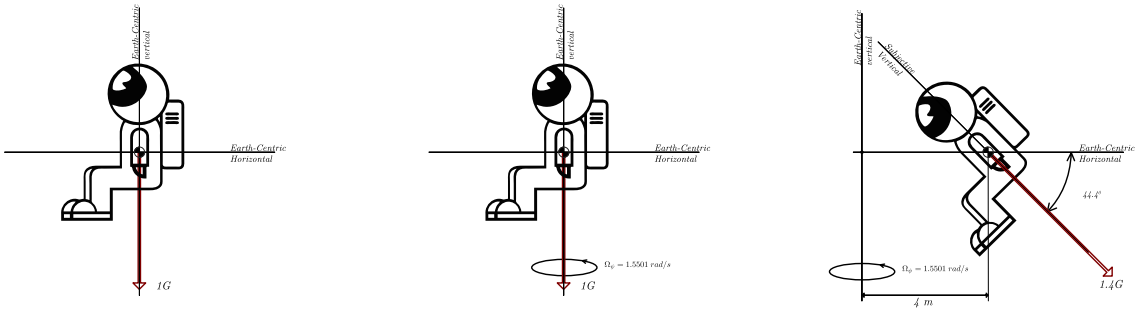

(a) Free body diagram of forces in 1G condition. Joe's upright is coincident to earth-centric horizontal and vertical.

(b) Free body Diagram of forces in 1Gyaw condition. Joe's upright corresponds to earth-centric horizontal and vertical orientation, however Joe is spinning around earth-centric vertical axis.

(c) Free body diagram of forces in 1.4G condition. Joe's upright is inclined at $44.4°$ **away from earth-centric vertical. additionally, Joe's center of mass is located 4 meters away from rotation axis. In combination with a central yaw spin, this results in elevated G-levels.**

Figure 10 Free body diagrams in upright position for three experimental conditions. Astronaut Joe represents the experimental subject situated inside Desdemona cabin.

Dependent Variables The dependent variables that were extracted from the experiment were the perceived tilt thresholds for roll and pitch in two directions. More specifically, the median, the Inter Quartile Range (IQR), the mean and the variance. Furthermore, in order to better understand the perception pattern, the frequency and combination of errors patterns in subject's answers was collected. The errors in this context is classified as inconsistencies in subjects answers regarding direction and/or axis of the perceived mismatch. Additionally, time traces of IMU data (gyros and accelerometer) were be collected and compared with commanded cabin angles.

4. Experimental Trials

The experiment consited of three gravitational conditions: 1 G with neutral (earth) gravity (C1), 1 G with yaw rotation (C2) and 1.4 G corresponding to a baseline G-level for F-16 cueing (C3). The free body diagrams for 3 experimental conditions is shown in Figure 10. Each participant was subjected to three experimental trials corresponding to the thee gravitational conditions and the starting order was randomized over all 12 subjects.The other two within factors, and thus conditions, are the axis (Pitch, Roll) and direction (+,-) having 2 levels each. Each tilt condition was repeated five times for each experimental trial. The order in which the tilts were presented, was randomized, resulting in $5 \cdot 4 = 20$ threshold measurements per trial. An overview of the tilt conditions in Table 1

5. Subjects

The participants, 12 naive subjects in total of mixed gender, 8 males and 4 females, and average age of 27 years were requited for this study. None of the subjects had prior experience in human centrifuges, three subjects were known to have prior experience with motion simulators and gliding experience. All of the subjects participated under their full consent and given the opportunity to withdraw at any time throughout the requirement. The methods and recruitment process used in the experiments were approved by the TNO's Toetsings-Commissie Proefpersoon-Experimenten (TCPE) experiment validation and subjects safety committee. Aside from three trials, each subject was given one practice session under 1G condition. The starting order in which the subjects were introduced to these G-conditions was varied randomly in order to exclude possible learning effects. Three conditions result in 6 possible combinations (3!), hence in total two blocks of 6 different orderings was distributed over these 12 subjects. The labels, A-F, corresponding to the starting order of the experimental trials is listed in Table 2.

Figure 11 Perceived tilt versus cursor presses convention used during the briefing of the participants.

Table 1 Overview of the independent variables (within factors) and corresponding levels.

IV's Levels	***Axis (P,R)*** [a]	***Direction (S)*** [b]	***G-Condition (C)***[c]
1	Roll	+ (RR or PU)	1G
2	Pitch	- (RL or PD)	1Gyaw
3	-	-	1.4G

[a] Axis levels: 1 = Roll, 2 = Pitch
[b] Direction levels: 1 = + (RR or PU) , 2 = - (RL or PD)
[c] G-Condition levels: 1 = C1 (1G), 2 = C2 (1Gyaw), 3 = C3 (1.4G)

6. Instructions & Procedure

Six wooden blocks with labels A-F were placed in a 'wizzards hat' and the subjects were asked to draw a label that determined their starting order. Once the hat was empty, the procedure was repeated until all the subjects were assigned a label. The result of the draw is shown in Table 2 in chronological order.

Each experimental trial consisted of 20 tilt measurements in total. Each tilt axis and tilt direction combination (roll right, roll left, pitch up and pitch down) as shown in Table 1, was measured 5 times. The subjects were introduced to these 20 random tilt angles and were asked to indicate the perceived tilt direction by means of a joystick input (forward=pitch down, backward= pitch up, left = roll left, right = roll right) as shown in the schematics in 11. Prior to start of each new run the subject was moved to the *'upright'*, corresponding to a perfectly upright seating position. The upright is the vertical plane parallel to the GIA at the start of the trial. The total travel of the cabin was limited to ±20° since no threshold measurements were expected above this level.

The upright was accompanied by a distinctive audio sound. Another sound registered the successful input of perceived tilt direction. Each trial corresponding to one of the 3 G-conditions took approximately 15 minutes depending on how fast the subject was able to register the tilts. For the course of three experimental trials, the participants were given a small break between the most demanding conditions (1.4 G and 1 G with a spin).

Table 2 Result of the draw for the starting order of the experimental trials. Subjects are listed in chronological order of participation.

Subject	1	2	3	4	5	6	7	8	9	10	11	12
Order	E	F	A	C	D	B	F	E	D	B	C	A

D. Motion Cueing

1. Cabin rotation

In this experiment it was necessary to avoid perceivable cabin rotations such that static body tilt threshold were establish on the basis of somatosensory and linear acceleration cues alone, without a contribution of the SCC. For this reason, the cabin rotations were carried out at, 0.4 degrees per second, below the sensory threshold levels for the angular acceleration and detectable t_{detec} levels associated with critical rotational velocity [27]. The Mulder product of 2.5 degree/s was used as the critical turnaround point below which the estimated detection time of acceleration steps is shown to approach infinity [27]. More explanation is given in Appendix D.

In addition the on-set of the commanded displacement of the cabin was rate limited and low-pass filtered to avoid acceleration peaks. Figure 12 shows a typical motion profile for a sequence of roll tilts. In the figure the rotational velocity during the acceleration phase, as well as during the constant phase stay below the critical velocity of 2.5 degree/s.

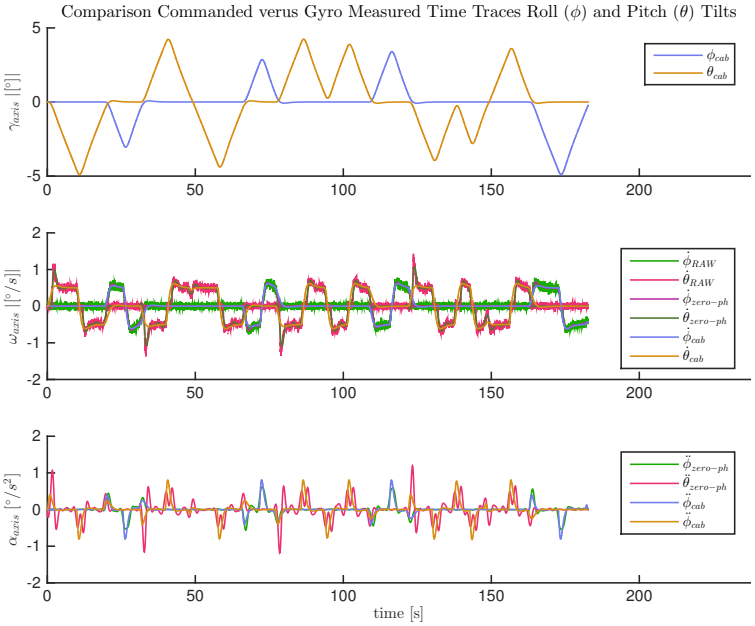

Figure 12 Time trace recoding of roll and pitch tilts. Comparison shows the commanded (yellow and blue) cabin angular velocity versus measured gyro velocity and filtered velocity at 0.5 $^\circ/s$.

Additionally the sequence of cabin roll and pitch rotations were analysed by means of the ACRM filter. The result of the analysis is shown in Figure 13a. Here the orientation of the cabin rolls corresponds to head-centric X (Roll) and Y (Pitch) Axes (see figure 4 for Holly's axis convention [7]). As seen, the filtered head-centric angular acceleration responses are below $1^\circ/s^2$ in all three head-centric axes. Based on ACRM response and considering the rotational velocity is kept below the Mulder product (2.5 degrees/s), the Coriolis rotations are expected to be undetectable by the human SCC's.

As a comparison of Coriolis rotation magnitudes, the deceleration phase (1.4G to 1G) of the centrifuge is shown in Figure 13b, for condition C3. While decelerating, the cabin pitch axis is rotated from the inclined 44.4° back to parallel position with the earth-centric vertical. As seen this produces larger magnitudes of the Coriolis Rotations (up to $5^\circ/s^2$) than during the sequence of cabin rolls. During this phase no experimental data were gathered.

2. G-cueing

For the conditions C1 and C2 every measurement started from the earth-centric level plane, assumed to correspond to the subjects upright. For both conditions C2 and C3, a constant yaw rotational component of 1.501 rad/s (88.814 $^\circ/s$) was present. In condition C3, once the steady-state 1.4 G-level was achieved, the roll and pitch angles were varied from the horizontal and the vertical planes corresponding to the orthogonal and parallel planes of the GIA inclined at an angle of $\theta_{align_{ss}} = 44.4^\circ$. The cabin attitude at the start of the trial in C3 condition was considered to be the 'new' subjective upright.

Both for C2 as C3, the measurements started at approximately 15 seconds after the transient, rotational (central yaw) and linear (tangential and radial) accelerations, had subsided.

Figure 10 shows the free body diagram of the exerted forces on the subject body for the three gravitational conditions at level position, with the 44.4 degree pitch angle alignment. Hence the equilibrium in this gravitational condition is actually inclined down from the earth-centric vertical.

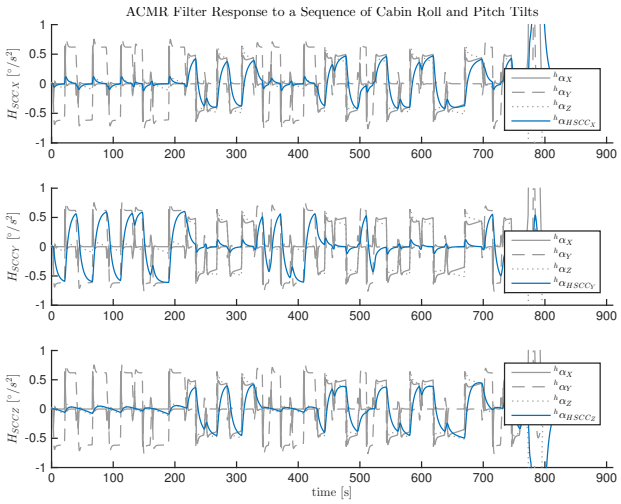

(a) ACMR model response to head-centric (X,Y,Z) accelerations during an actual sequence of cabin roll and pitch tilts (angular velocity is 0.4 $^\circ/s$) in experimental condition C2 (1.4 G-level under centrifuge rotation of $\Omega_{\psi_{SS}} = 1.5501$ rad/s). The ACMR filter is based on holly's kinematic model [7] and Hosman et al. SCC filter model [14]. The Whole-Body rotations occur around head-X (Roll) and head-Y (Pitch) axes.

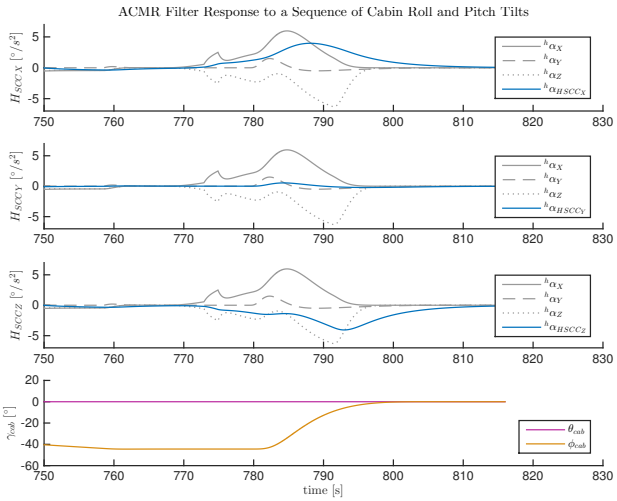

(b) ACMR model response to head-centric (X,Y,Z) accelerations during cabin pitch alignment and centrifuge deceleration phase from 1.4 G to 1 G level. No threshold data is gathered during this phase

Figure 13 ACRM analysis of the commanded sequence of cabin roll and pitch cues.

V. Results

A. Statistical Analysis Method

Sample data gathered from the subjects were analysed using MATLAB and SPSS. For the statistical analysis, a three-way Repeated Measures Analysis of Variance (Repeated Measures ANOVA) was conducted to compare the effect of the within factors, Axis, Direction and G-Condition. The result of the Repeated Measures ANOVA is shown in Table 3. The within factors, or repeated measures factors, had the respective levels, 2 (Roll,Pitch), 2 (+,-) and 3 (C1,C2,C3). An overview of the factors and corresponding levels is given in Appendix C in Table 8. The rightmost column in the table contains the labels corresponding to the within factor combinations. The latter is also the source variable used as the column input in SPSS and MATLAB.

Each tilt (RR,RL,PD,PU), or Axis·Direction combination, was measured five times (N=5) for the three experimental trials, totaling $2 \cdot 2 \cdot 5 \cdot 3 = 20$ observations per subject. The sample data input for the Repeated Measures ANOVA test was the mean of the 5 observations measured per subject and per combination. The resulting (nxm) sample data matrix consisted of, $n = 12$ rows of repeated measures from 12 subjects, and $m = 2 \cdot 2 \cdot 3 = 12$ within factor combinations as columns as listed in the rightmost column of table 8. No statistical analysis was performed to study the order effects A-F. The purpose of randomising the starting order was to eliminate the learning effects.

Furthermore several supportive tests were conducted in order to verify the validity of the sampled data and the justification of the statistical method. The series tests showed that the sample data met the normality, reliability and Sphericity tests required for parametric test such as the Repeated Measures Anova. A hystogram overview of the results is presented in Figures 14 and a tabular overview in Appendix B and Appendix B.

1. Outliers in Sample Data

The outliers were classified and extracted from the box-plots presented in the results section, however, these data points were not excluded from the statistical analysis. For the graphical representation mean data was calculated and the outliers were labeled as separate data points. This was required to ensure that no information was lost that otherwise may point out possible (hidden) relationships between factors.

For the 12 subjects, the mean and the standard deviation; the median and the IQR was calculated from the five

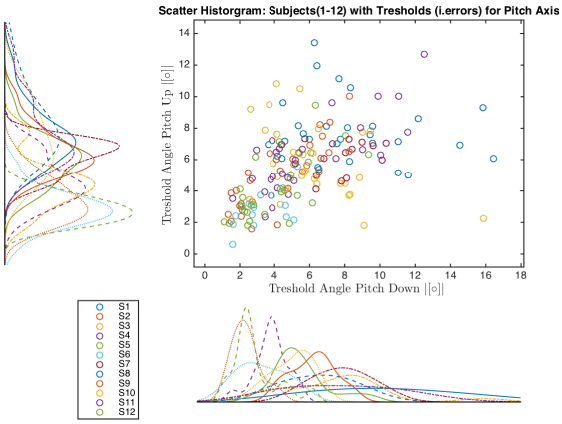

(a) Scatter histogram of threshold observations: Comparison of direction levels (PD,PU) for 12 subjects.

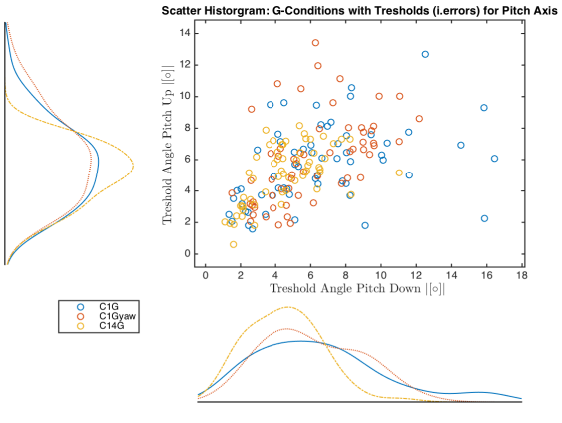

(b) Scatter histogram of threshold observations: Comparison of Direction levels (PD,PU) for conditions C1, C2 and C3.

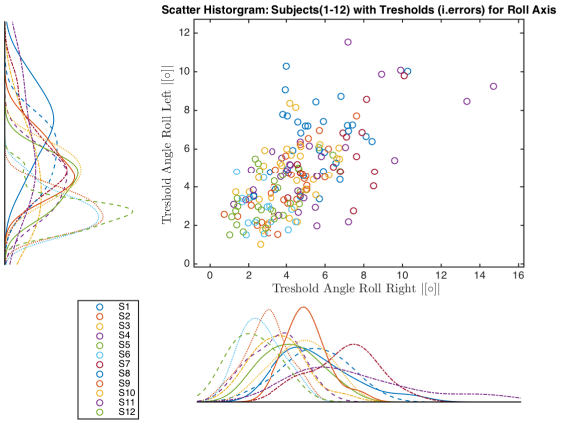

(c) Scatter histogram of threshold observations: Comparison of Direction levels (RR,RL) for 12 subjects.

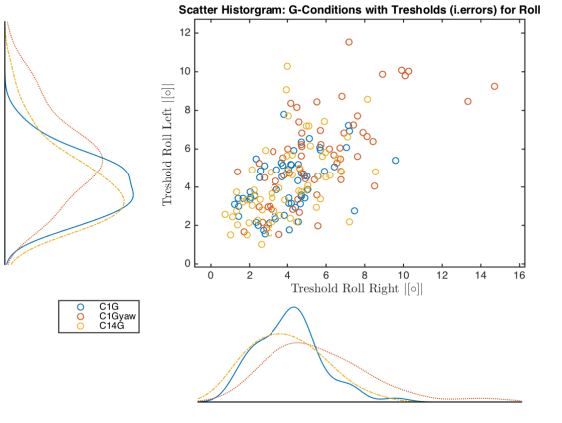

(d) Scatter histogram of threshold observations: Comparison of Direction levels (RR,RL) for conditions C1, C2 and C3.

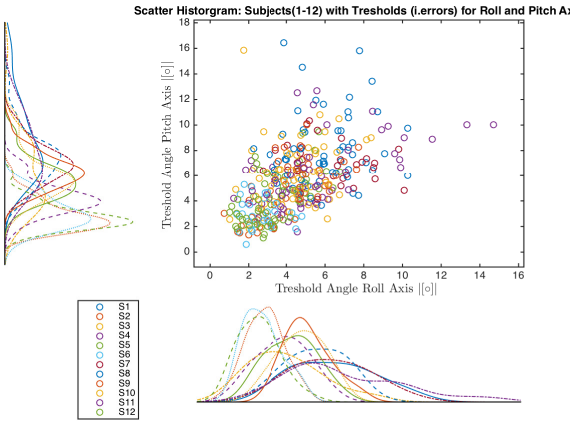

(e) Scatter histogram of threshold observations: Comparison of Axis levels (R,P) for 12 subjects.

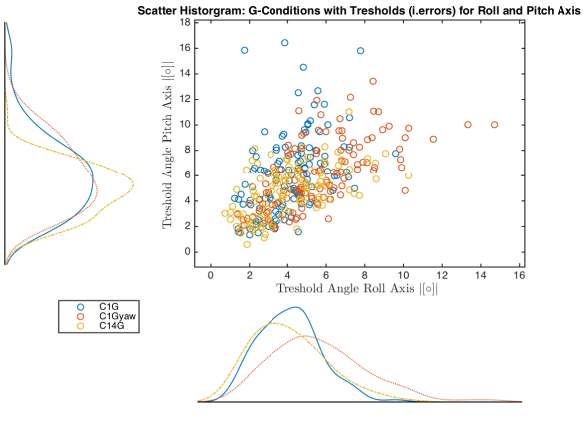

(f) Scatter histogram of threshold observations: Comparison of Axis levels (R,P) for Conditions C1, C2 and C3.

Figure 14 Scatter histograms of threshold data organized per subject and per trial for comparison of Axis, and Direction Levels.

Table 3 Repeated measures three-Way anova results. Within factors: Axis (Roll,Pitch), Direction (+,-) and G-Condition (1G, 1Gyaw, 1.4G).

Measure					
Source	Type III Sum of Squares	df	Mean Square	F	Sig.
Axis	40.435	1	40.435	23.248	0.001
Direction	0.002	1	0.002	0.001	0.977
Gcondition	51.390	2	25.695	13.276	0.0002
Axis · Direction	0.461	1	0.461	0.154	0.703
Axis · Gcondition	15.597	2	7.798	6.733	0.005
Direction · Gcondition	3.784	2	1.892	2.329	0.121
Axis · Direction · Gcondition	2.460	2	1.230	2.281	0.126

repeated observations of the perception thresholds values. This was done for 4 Axis·Direction combination over all three experimental trials, namely the 1G, 1Gyaw and the 1.4G. The calculation was performed both for the data set containing the errors in tilt reports, indicated as *Including Errors*, and the data set excluding the errors, identified as *Excluding Errors*. The incorrectly reported tilts are those that do not match, in either direction, axis or both, to the actual tilt that the participants are subjected to. An overview of the error reports is given in Appendix A.

A series of box plots was made for the two sets, to visualize the difference in thresholds values obtained from the sample data presented in figs. 15a, 15b, 16a and 16b and fig. 16. Additionally an overview of the data is given in tables 4 and 5. The tables, likewise come in two sets, with and without errors. Tables are made for median and IQR values; mean and Standard Deviation (SD)values; adjacent values, and finally, the outliers occurring in the data. All of these values are sorted per twelve possible combinations of axis, direction and Condition. Values corresponding to independent factor combination that contained errors throughout the $N = 5$ observations are indicated in bold.

In the box plots, the median is indicated by a colored dark horizontal line inside the filled rectangular area. The bottom and top edges of the rectangular boxes indicate the upper and lower quartiles (25th and 75th percentile). The adjacent range, indicated by the upper and lower whiskers is the range of extreme data points excluding the outliers as summarized in Table 6. In order to show a representative overview of the perceived thresholds, the outlier values, shown in Table 7 were extracted from the data set and marked with a red plus sign, '+' on the box plots. These values were, however not excluded from the statistical analysis for the reasons explained in section V.A. A data point x_i was labeled as an outlier under the following condition:

$$\left.\begin{array}{ll} x_i & < q_1 - w(IQR) \\ x_i & > q_3 + w(IQR) \end{array}\right\} = x_{outlier} \tag{6}$$

Here $q1$ and $q3$ represent the 25th and 75th percentiles, and the IQR, inter quartile range $q3 - q3$, respectively. The w represents the default whisker width of 1.5, that corresponds to $\pm 2.7\sigma$ and 99.3 percent coverage for normally distributed data [29].The data set including errors does not contain additional outliers, meaning that none of these incorrectly perceived tilts meet the conditions to be labeled as outliers and hence lie within the adjacent range. In order to show the spread of these errors, these data points were plotted separately on each respective axis and direction and labeled as 'o'.

2. Main Effect Axis: Differences Roll and Pitch

The differences for axes, Roll and Pitch are clearly evident in the comparison plot in fig. 15a. Here the threshold data has been bundled across G-conditions and directions yielding a comparison between the two Axis levels, R and P. The Roll axis (Roll R, Roll L) shows the lowest median thresholds, this holds for data set including and excluding the perception errors. The values are, (4.491, 4.530), (5.305, 5.288) for Roll and Pitch, respectively. The respective mean values are (4.603, 4.662), (5.652, 5.640). Likewise, the variance found in Roll Axis is clearly lower compared to pitch. This is shown by the respective IQR, (2.680, 2.587), (3.450, 3.442), and the SD (2.154, 2.145), (2.710, 2.710), values. Likewise, the adjacent range is much higher for Pitch compared to roll with values (max,min) , (9.59, 0.611), (12.16, 0.61), for Roll and Pitch, respectively.

The statistical analysis confirms these findings, showing a highly significant main effect for Axis ($F = 23.248$; d.f. $= 1$; $p < 0.005$).

The impact of the errors in the data set is minimal as shown by the values comparing the set with and without errors. There is a small difference in the adjacent range for Roll axis, 0.0726 versus 1.1014, for errors vs no errors. As seen in the graph, the scatted error values remain in the adjacent range and do not produce significant outliers.

Comparison axis-wise thus suggest that the Roll tilt is less ambiguous compared to Pitch tilt. In other word the subjects tend to identify GIA Roll mismatch quicker and more accurately, as suggested by the lower threshold and spread shown in Fig. 14e and 15a.

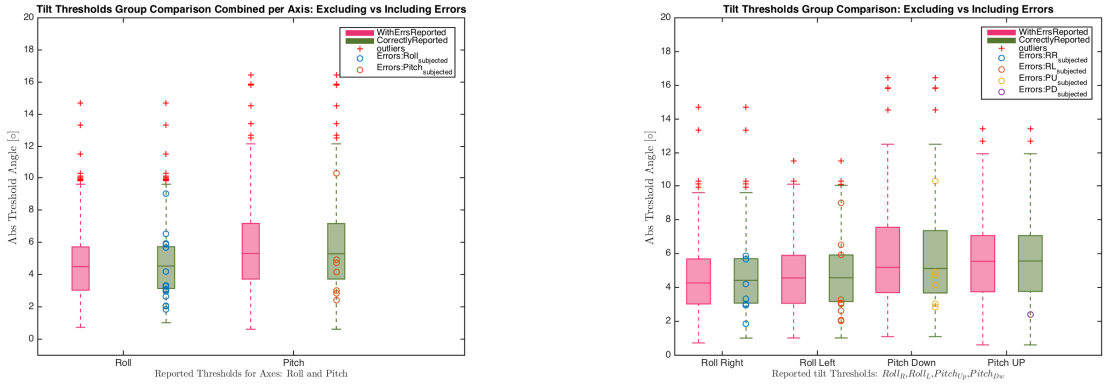

(a) Comparison of group median thresholds for Axis, including and excluding Errors. Perception errors to subjected tilt are plotted separately on corresponding Axis.

(b) Comparison of group median thresholds for Axis and Direction, including and excluding Errors. Perception errors to subjected tilt are plotted separately on corresponding Axis and Direction.

Figure 15 Comparison of group median thresholds, including and excluding errors.

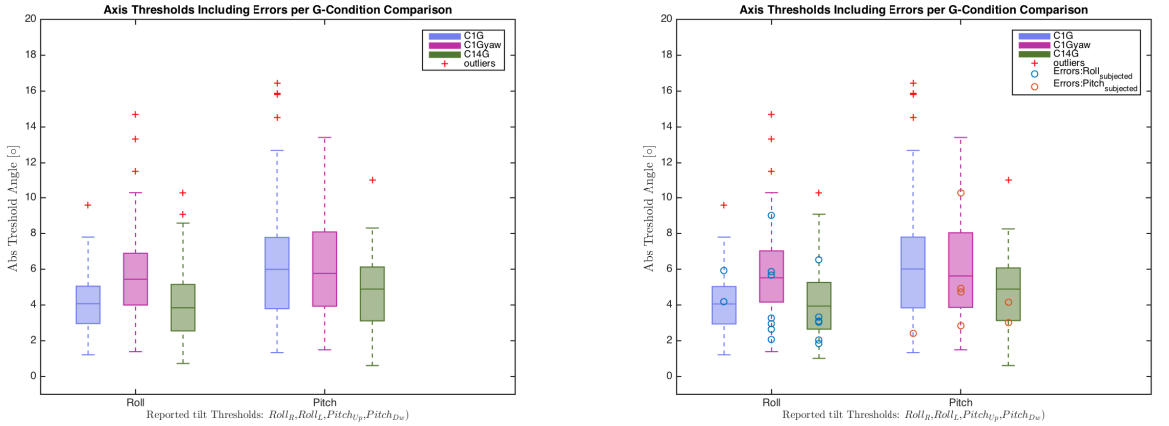

(a) Boxplot of median tilt threshold values including errors for combined Axis (Roll and Pitch) and G-Condition.

(b) Boxplot of median tilt threshold values excluding errors for combined Axis (Roll and Pitch) and G-Condition. perception errors to subjected tilt axis tilt are plotted separately on corresponding the Axis.

Figure 16 Group mean perceived tilt thresholds for all conditions and subjects.

3. Interaction Effects G-Condition vs Direction

The interaction between the gravitational condition and axis direction was highly non significant (F = 2.329; d.f. = 2; p > 0.05). The statistical analysis also showed that no main effect was present as for factor direction as seen previously. This suggests that there is a certain symmetry between positive and negative, that hold across both the G-conditions (C1-C3) as the Axes (Roll,Pitch). Examining the hystogram overview and figures 17a and 17b. The symmetry seems to hold for C2 and C3, however, visually Pitch Down and Pitch Up seems to show asymmetry in C1. This points to the discrepancy in statistical results compared to visual inspection. Knowing that for the statistical test, the mean data was used instead of the median data, a comparison of numeric values for three way interaction given in tables 4 to 6, is useful. Comparing the mean (PD,PU), (6.512,5.657) and median (6.182,5.803) values; the SD (3.691,2.488) and IQR (4.400,3.369) it is evident that the discrepancy is not due to the difference in two measures used. The adjacent range seems to support the discrepancy found in this particular case, the PD vs PU clearly shows a much higher range. It also shows quite extreme outliers compared to PU. Visual inspection thus suggest in this case that there is quite a difference in perception of PD versus PU, whereas the statistical test disagrees. Put it differently, the visual investigation points out that the mismatch in PD is more ambiguous compared to PU. For the other cases C1 and C2 the symmetry generally holds.

The ambiguity in Pitch Down can also be confirmed by the nominal distribution, shown in the scatter histogram in Figure 14f. The threshold observations of PD are scattered across a larger interval ($\approx [1-17]^\circ$) compared to PU ($\approx [1-14]^\circ$).

One other important thing to note is the difference in numerical values for C2 in PD vs PU. Comparing the mean (PD,PU), (6.098,6.089) and median (5.458,6.281) values, thee is a clear asymmetry in median while there is almost none in mean. This is also true in roll (RR,RL), (4.638,5.647) and median (4.873,5.573). The latter likewise suggests that the visual inspection would point out asymmetry in C2 in directions RR versus RL. Difference are smaller compared to PD-PU discrepancy in C1.

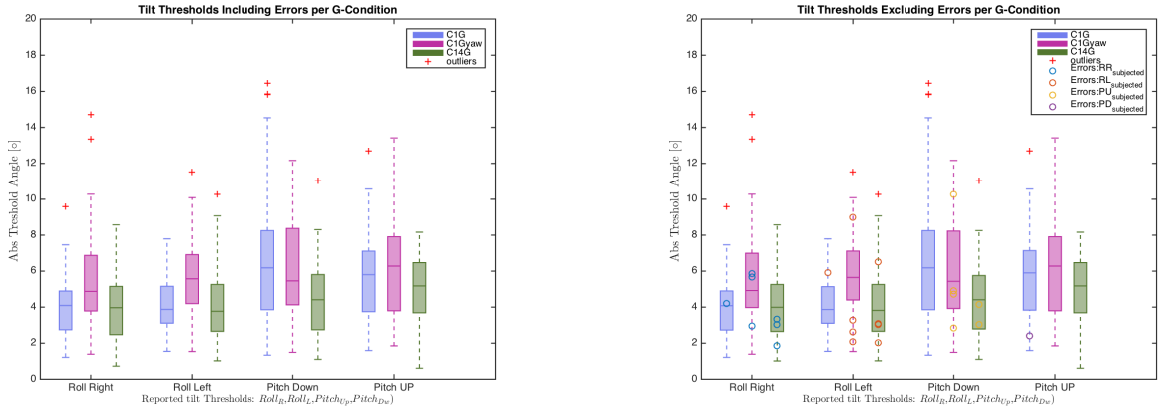

(a) Boxplot of median tilt threshold values including errors per Axis, Direction and G-Condition.

(b) Boxplot of median tilt threshold values excluding errors per Axis, Direction and G-Condition. Perception errors to subjected tilt are plotted separately on corresponding the Axis, Direction and G-Condition.

Figure 17 Group mean perceived tilt thresholds for all conditions and subjects.

4. Three-Way Interaction

The statistical test of the three-way interaction did not show significance. Visual inspection for this interaction is perhaps the hardest to judge, however, as pointed out in the previous section, the particular combination C1PD jumps out with the highest median and adjacent range.

Figures 21a and 21b give an overview of the percentage of errors encountered in repeated factors (within factors), these are the G-condition, Tilt Axis and Tilt Direction. The bar plot for the G-Condition, shows that C2 and C3 show the highest concentration of errors, 4.58 and 3.75 %, respectively. 1G condition shows the lowest concentration of errors with only 1.25%. Roll axis shows the highest concentration of errors in (RR,RL), 3.9 and 5 %, respectively. Pitch axis shows least amount of errors, 3.33 and 0.56, respectively, with the direction PU having the absolute lowest error

percentage.

It is also interesting to see the correlation between the exact combination of the perceived and the actual tilt. Bar plot 20a shows how the actual tilt was perceived when reported wrongly. It is evident that combination RR_{perc}-PU_{act} has the highest occurrence.

The exact percentage of errors per subject for all three trials is shown in figure 21c. Labels A-F indicate the starting order of the experimental G-Condition, occurring twice for each set of 6 subjects. Subject number 12 (order B) shows significantly higher percentage of errors in all three conditions compared to the group, with in total 7 occurrences of errors (out of 20 measurements times 3 G-Conditions). Subjects 7-11 with labels, B,E,F and A show no errors at all.

VI. Discussion

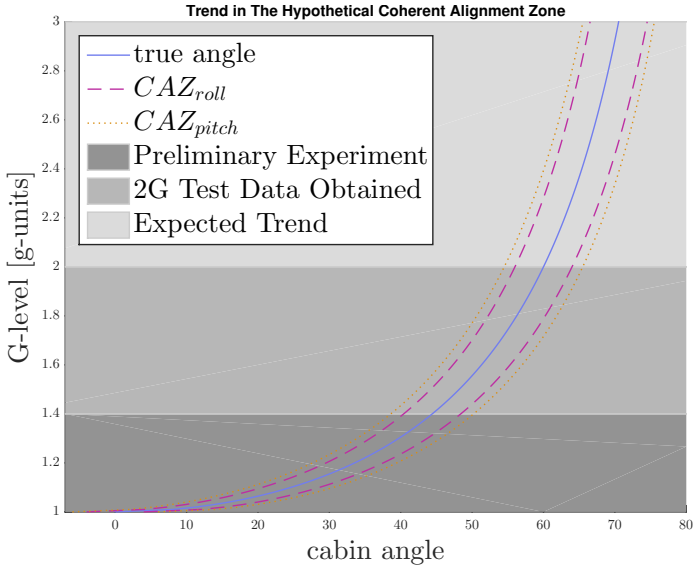

Figure 18 Coherent Alignment Zone in pitch coordination showing the obtained data and expected trend for g-levels 1-3 [3].

This study set out to establish human perception thresholds for Roll and Pitch tilt. An attempt was made, to investigate the effects of the gravitational environment (G-Condition). The latter was done by arranging the G-conditions in three experimental trials, normal 1G gravity condition (C1), normal 1G with central yaw rotation (C2), and lastly elevated gravitational condition at 1.4G level (C3). During these trials, participants were subjected to four body tilts (RR,RL,PU,PD) varying in axis, Roll and Pitch, and direction, positive (RR or PD) and negative (RL or PU). Their task was to identify the mismatch with respect to the resultant gravitational vector, solely relying on the somatosensory and static linear acceleration cues, in the absence of any visual input. The effect of gravitational condition was an important factor to be investigated, however, the crux of this study was to either confirm or reject the initial belief that there is an instinctive and significant difference in the manner by which Roll and Pitch tilts are perceived in terms of body-G-vector mismatch.

As the statistical analysis shows, a significant difference in perception of roll and pitch mismatch is believed to exist. Remembering the hypothesis, namely the differential versus absolute sense of mismatch, the findings seem to be supportive in this regard. For this reason, roll tilt is believed to produce a differential stimulus across the saggital (vertical) body axis, where one side of the seat and head rest exerts higher pressure compared to the other. Due to this relative pressure interface, Roll is believed to be easier to decode into a sense of GIA mismatch. In contrast no differential interface exist in Pitch. There is a pressure point on the back of the head and head rest interface, and the interface along the back of the spine and bottom, however no interface is present on the front plane of the body. Naturally, the judgment of mismatch during body tilt, from the somatosensory cues can only be compared to the same absolute pressure interface before and after the tilt. In fact the mechanism is a continuous process. The pressure dissipation of the absolute point is continuously evaluated across interval $[t_0 - t_1]$ against the reference pressure value estimated at

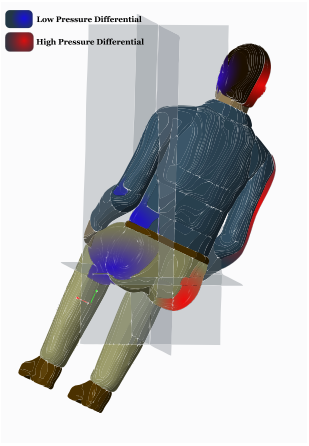

(a) Differential Pressure Interfaces Mechanism Roll Tilt. The Somatosensory Cues are Compared at Opposite Differential Points Along The Symmetry Axis. Red and Blue Regions Indicate High and Low Pressure Points Respectively.

(b) Absolute Pressure Interface Mechanism Pitch Tilt. No Differential Pressure Points are Present for Pitch. Rather, the Somatosensory Cues Are Continuously Evaluated for interval $[t_0 - t_1]$ at an Absolute Pressure Point Against Reference Point (head rest) at $t = t_0$. The Yellow Region Indicates Time Dependent Dissipating Pressure Region.

Figure 19 Difference in threshold determination for Pitch and Roll Axes.

time $t - t_0$. This makes the process much more ambiguous. Additional explanation is given in figure 19 along with the illustration.

A possible intuitive explanation for this difference can perhaps be attributed to our body's natural preference for body orientation with respect to gravity. It could very well be that when our body is held sideways, we get an immediate sense of action and perhaps also a sense of discomfort and danger. For example, from experience we know that when we tilt sideways in a chair we are more likely to tip over and fall, whereas we are much more reckless when tipping the chair backwards. Similarly, being tilted sideways in a car or a motorcycle has an imminent sense of action happening. Therefore, it is not hard to believe that our body must have developed a certain preference and accuracy for a particular orientation. To further this logic, our findings show that a symmetry is found direction wise. The latter was also confirmed in the study of Beuzekom et al., although the tilt angles were much higher [22]. While this strongly supports the logic regarding sideways roll, it invalidates this specific reasoning regarding pitch. If the symmetry would hold in pitch, then naturally, the absence of a second pressure interface apposite the backside of the chair should not be of importance. However, perhaps it so happens, that this absolute interface in Pitch is calibrated nearly equally for Forward and Backward tilt. It is important to note, however, that the discrepancy found in the visual and statistical analysis, points out prior logic indeed should get the benefit of the doubt. This intuitive existence of symmetry-asymmetry in Roll and Pitch was also confirmed by estimation models of Clark et al. in a recent study [30].

The other major finding was the expected trend of lower thresholds for higher GIA resultant. Thinking again in terms of somatosensory stimulus, higher gravitational resultant vector should naturally result in higher pressure stimulus across the roll and pitch interfaces, thusly, making the judgment of tilt less ambiguous. Its must be noted that this was more so in case of pitch tilts, roll tilts showed little difference across C1 and C3. A possible explanation could be that the differential interface estimator cannot be further exploited as it is calibrated for the relative pressure stimulus. As the magnitude of the G-level changes, the relative pressure difference between the differential interfaces during roll tilt for C1 and C3 is almost unchanged. In other words the relative change across two interfaces (decrease in pressure stimulus from one side and increase of pressure stimulus to other side) after roll tilt from the initial upright, is in the same order of magnitude as during C1. Moreover, the differential interfaces could be already well calibrated, thus allowing much less gain in accuracy. Since the pitch interface is absolute in nature, the increase in GIA magnitude should accommodate for more accuracy and effective.

Another aspect that may have played a significant role in this condition is the contribution from the otoliths. As explained in Appendix D the detection time of linear acceleration shows a certain resolution in acceleration steps [27]. It is believed that, due to increase in the magnitude of the GIA, T_{detect} was significantly dropped, such that the otolith-estimator contributed to a more accurate judgment of the mismatch. As hypothesized earlier, the findings

regarding the the variance and the threshold levels support this claim.

If the trend is believed to hold across increasing G-levels, this would mean that the expected Coherent Alignment Zone should narrow down. However, discomfort and strain experienced from elevated G-levels may affect the subjects judgments of the GIA mismatch, and cause the trend to keep steady or diverge again. For most subjects, the strain to keep an upright posture, starts to become noticeable at G-levels of 2 and above. To fully confirm these post-hypotheses, additional experiments wold be required.

A peculiar side effect of the trials involving the central yaw rotation (C2 and C3) was the increased number of perception errors as shown by the graphs 21a,21b and 21c. Although no statistical analysis was performed to prove or disprove this relationship, the majority of the subject reported that for trial C2 the perceived tilt was often ambiguous. The roll tilts in particular seemed to have a coupling effect, RR perceived as PU, PU perceived as RL and RL perceived as PD. Collected error data agrees with the subjects experience, shown by 3D bar plot of the perceived and actual tilt pairs (figure 20a). The afore mentioned combinations indeed have the highest occurrence. This seemingly systematic errors may have a possible reasons. The errors in perception may be attributed to Coriolis cross coupling effects. Obviously, pure yaw rotation in the earth-centric vertical plane should not cause any passive Coriolis effect considering the subject does not make any rotations outside this rotational plane, however, its is worthwhile to consider what would happen if the person would make head movements. Taking as example the most extreme case, where, as described in the rotating platform experiment by Guedry [10], the subject would initiate a rightward 30 degree head tilt in during constant rotation (vector pointing upward). The resultant angular vector producing simultaneous canal stimulus and the misalignment with the signal from the otolith about the Subjective Vertical (SV) would trigger a significant Coriolis Effect and a sensation of tumbling forward. In the less extreme case this would be a sensation of pitching down. This reasoning seems to confirm the effect of coupling in the errors. The question remains, how the head tilt is initiated when the subjects are not supposed to move. Of course leaving the trivial case of a subject deliberately moving his head around, the latter could have two reasons. Firstly, the 'head movement' may be caused by the disturbance introduced due to yaw rotation. The central (main) yaw track is known to contain a slight bump and cause vibrations along the G_z. Secondly, the head tilt may be initiated by the subject himself, although not intentionally, causing the coupling effect. When considering sideways tilt (Roll) in relation to our body's responses, instinctively, our body wants to correct itself and move away from this uncomfortable position back to the vertical upright. However, as the subject is strapped no body movements are possible, this leave the possibility to compensate with a head tilt in the opposite direction. Although, the head sits in the headrest, a limited range of motion is available (and likely to happen), presumably resulting in couples experience of body-tilt. In summary this two effect could be possible causes. However, it is not possible to formally prove the existence of the coupled effect with this limited amount of measurements, this is be a matter that requires more investigation and experimental trials. Furthermore, 1G yaw rotations rotations at velocity level of 1.4G levels and above, do not have a realistic and practical use case in G-cueing, aside from fundamental rotating platform experiments.

1. Concluding Remarks

Viewing these findings from a higher vantage point, this study suggest the following important remark, namely, that perception of the mismatch of GIA misalignment is not a straightforward discrete process. Rather, the perception process is a continuous evaluation of immediate (faster) sensory stimulus and intermediate estimations of ones orientation. The threshold in this context, can be characterized as a narrow region of tilt angle interval that has a high probability of being classified and perceived mismatch. The exact point at which this occurs is ambiguous, an depends on the many feedback and decision loops that compose this estimation process. This is illustrated in Fig. 20. Hence, claims should not be made regarding the exact limits of Pitch or Roll thresholds, but rather likelihood of coherent regions and decrease in ambiguity. In other world for practical applications of these threshold limits, one should define approximate regions of coherency with respect to GIA alignment, instead of using hard limits.

VII. Conclusions

This study attempted to answer in which orientation (Pitch or Roll) subjects are less sensitive to specific force direction errors. The hypothesis was that the pitch-axis would result in higher tilt thresholds due to differences of somatosensory pressure interfaces stimulated with pitch or roll tilt.

The main results of this study, and the established CAZ-region are shown in Figure 15a and 18. The findings of the experiment supported the hypothesis that pitch has a higher ambiguity, by showing higher treshholds and spread for pitch versus roll ($\approx$ 6 versus $\approx$ 4 degrees) [3]. The higher threshold and ambiguity in pitch, suggested that the COHAM has more 'room' to operate in the pitch-axis, and so cabin motion could be minimised to a greater extent due to the

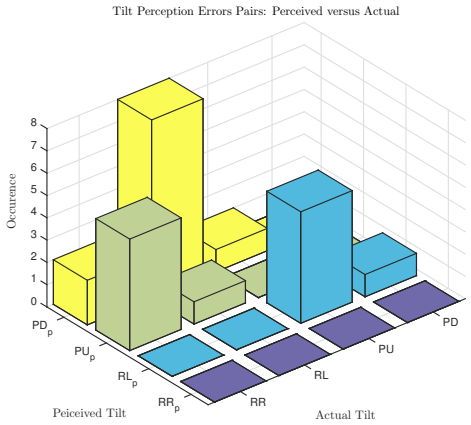

(a) 3D Bar Plot of Tilt Perception Error Pairs. The Perceived Tilts are Subscripted with $_p$.

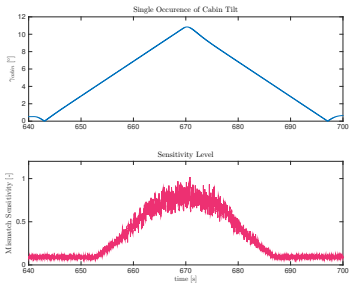

(b) Illustration of Perceptual Ambiguity of GIA Mismatch. The Bottom Plot Shows a Hypothetical Time Trace of Mismatch Sensitivity during 700 second Angular Cabin Travel of 0-10°. The Mismatch is not perceived at a particular point in time. Rather, actual cabin tilt has a high probability of being perceived as mismatch within a narrow band of cabin angle excursion. within this band the mismatch is continuously evaluated until the sensitivity peaks and a subject has full certainty about mismatch and the corresponding direction.

Figure 20 Perceptual ambiguity of tilt mismatch and overview of error reports

larger CAZ region in pitch, thereby reducing the Coriolis effect. For this reason, pitch was found to be more suitable for the COHAM and this study recommended continuing the development of the COHAM-filter (with a 5 degree pitch mismatch).

The COHAM filter was suggested to be tested with static CAZ first, prior to incorporating the trend expected from the experiment data, shown in Figure 18. Static CAZ is defined as coherent alignment region that has fixed values irrespective of G-level. The trend in 18 established by the experiment showed that thresholds potentially are expected to decrease with higher G-levels. It was therefore suggested to extend the validation set of CAZ to higher G-levels. Using this data a dynamic CAZ region could be defined, where the threshold actively varies with the G-level (i.e. shrinks and expands).

A possible cause of the difference observed in the pitch and roll axes was suggested to be due to the difference of somatosensory pressure interfaces. It is believed that subjects 'measured' roll misalignment using a differential pressure interface (left and right side of the body along the symmetry axis), providing immediate comparison between pressure differences. The pitch misalignment, on the other hand, was believed to be measured using absolute (time dependent) somatosensory cues, where the pressure cues were sampled from a dissipating pressure region (backside of the head and back), and compared against an absolute reference point (head rest at $t = 0$) for the duration of the tilting motion. The latter was believed to lead to higher ambiguity in pitch axis, making it harder to 'perceive' the tilt. This is schematically illustrated in Figures 19a and 19b. Additional experiments are suggested to confirm this reasoning.

Furthermore, this study suggest to conduct a follow-up study, focusing more on a 'dynamic process' of body tilt perception. Current experiment was designed to establish perceptual body tilt threshold mainly from a static point of view. This was done with very slow rotations and largely relying on somatosensory, with a small contribution from the otoliths and no contribution from the SSC. A possible approach would be to use these 'freshly obtained' threshold values, an directly carry out another sub experiment involving dynamic oscillations between the positive and negative (Roll or Pitch Axis). Another potential addition would a similar experiment in combination with 'active threshold tuning'. The active tuning approach has been used in another study in determining phase coherence zones between yaw rotation and a visual reference [13].A possible method for active tuning could be a type of nulling method used in early studies [27]. However, this may involve addition complexity in the estimator dynamics. Furthermore, the elevated G-levels used for the experiment are believed to have a strong impact on the detection time, adding to the complexity of estimator dynamics and spread in the subjects results.

References

[1] Burton, R. R., "G-induced loss of consciousness: definition, history, current status." *Aviation, space, and environmental medicine*, 1988.

[2] Creer, B. Y., Smedal, H. A., and Wingrove, R. C., "Centrifuge study of pilot tolerance to acceleration and the effects of acceleration on pilot performance," 1960.

[3] T.Mkhoyan, "Minimisation of Coriolis Effect in Human Centrifuges: Preliminary Study," unpublished.

[4] Roza, M., Wentink, M., and Feenstra, P., "Performance testing of the desdemona motion system," *AIAA modeling and simulation technologies conference and exhibit*, 2007, p. 6472.

[5] Schubert, G., *Die physiologischen Auswirkungen der Coriolisbeschleunigungen bei flugzeugsteuerung*, J. Springer, 1932.

[6] Guedry Jr, F. E., "Psychophysics of vestibular sensation," *Vestibular System Part 2: Psychophysics, Applied Aspects and General Interpretations*, Springer, 1974, pp. 3–154.

[7] Holly, J. E., "Subject-coincident coordinate systems and sustained motions," *International Journal of Theoretical Physics*, Vol. 35, No. 2, 1996, pp. 445–473.

[8] Holly, J. E., Vrublevskis, A., and Carlson, L. E., "Whole-motion model of perception during forward-and backward-facing centrifuge runs," *Journal of Vestibular Research*, Vol. 18, No. 4, 2008, pp. 171–186.

[9] Holly, J. E., "Vestibular coriolis effect differences modeled with three-dimensional linear-angular interactions," *Journal of Vestibular Research*, Vol. 14, No. 6, 2004, pp. 443–460.

[10] Guedry, E. and Benson, A., "Coriolis cross-coupling effects: disorienting and nauseogenic or not?" *Aviat Space Environ Med*, Vol. 49, 1978.

[11] Desdemona, "Welkom to Desdemona eu," `http://www.desdemona.eu/`, 2010, [Online; accessed 2-July-2017].

[12] van der Steen, F. A. M., *Self-motion perception*, Ph.D. thesis, TU Delft, Delft University of Technology, 1998.

[13] Valente Pais, A., *Perception Coherence Zones in Vehicle Simulation*, Ph.D. thesis, TU Delft, Delft University of Technology, 2013.

[14] Hosman, R. and Van der Vaart, J., "Vestibular models and thresholds of motion perception. Results of tests in a flight simulator," *Delft University of Technology, Department of Aerospace Engineering, Report LR-265*, 1978.

[15] Tribukait, A. and Eiken, O., "Perception of the head transversal plane and the subjective horizontal during gondola centrifugation," *Attention, Perception, & Psychophysics*, Vol. 67, No. 3, 2005, pp. 369–382.

[16] Tribukait, A., "Semicircular canal and saccular influence on the subjective visual horizontal during gondola centrifugation," *Journal of Vestibular Research*, Vol. 9, No. 5, 1999, pp. 347–357.

[17] Tribukait, A. and Eiken, O., "Roll-tilt perception during gondola centrifugation: influence of steady-state acceleration (G) level," *Aviation, space, and environmental medicine*, Vol. 77, No. 7, 2006, pp. 695–703.

[18] Tribukait, A., Bergsten, E., and Eiken, O., "Variability in perceived tilt during a roll plane canal-otolith conflict in a gondola centrifuge," *Aviation, space, and environmental medicine*, Vol. 84, No. 11, 2013, pp. 1131–1139.

[19] Tribukait, A., "Human vestibular memory studied via measurement of the subjective horizontal during gondola centrifugation," *Neurobiology of learning and memory*, Vol. 80, No. 1, 2003, pp. 1–10.

[20] Mast, F. and Jarchow, T., "Perceived body position and the visual horizontal," *Brain research bulletin*, Vol. 40, No. 5, 1996, pp. 393–397.

[21] Mittelstaedt, H., "The subjective vertical as a function of visual and extraretinal cues," *Acta psychologica*, Vol. 63, No. 1, 1986, pp. 63–85.

[22] Van Beuzekom, A. and Van Gisbergen, J., "Properties of the internal representation of gravity inferred from spatial-direction and body-tilt estimates," *Journal of Neurophysiology*, Vol. 84, No. 1, 2000, pp. 11–27.

[23] Clark, B. and Stewart, J., "Coriolis effects during pitch and roll maneuvers in a piloted flight simulator," 1964.

[24] Moore, S., Cohen, B., Clément, G., Curthoys, I., Dai, M., Koizuka, I., Kubo, T., Raphan, T., Moore, S., Curthoys, I., et al., "Ocular counter-rolling during centrifugation and static tilt," *The Neurolab Spacelab Mission: Neuroscience research in Space. NASA SP-2003-535*, 2003, pp. 11–17.

[25] Tarnutzer, A. A., Bockisch, C., Straumann, D., and Olasagasti, I., "Gravity dependence of subjective visual vertical variability," *Journal of neurophysiology*, Vol. 102, No. 3, 2009, pp. 1657–1671.

[26] Schöne, H. and De Haes, H. U., "Perception of gravity-vertical as a function of head and trunk position," *Zeitschrift für vergleichende Physiologie*, Vol. 60, No. 4, 1968, pp. 440–444.

[27] Young, L. R., "Perception of the body in space: mechanisms," *Comprehensive physiology*, 1982.

[28] Mann, C. and Dauterive Jr, J., "The Perception of the Postural Vertical: I, The Modification of Non-labyrinthine Cues," Tech. rep., Joint Report.

[29] MATLAB, "MATLAB boxplot documentation," `https://nl.mathworks.com/help/stats/boxplot.html`, January 2017.

[30] Clark, T. K., Newman, M. C., Oman, C. M., Merfeld, D. M., and Young, L. R., "Modeling human perception of orientation in altered gravity," *Frontiers in systems neuroscience*, Vol. 9, 2015.

[31] Cramer, D., *Fundamental statistics for social research: step-by-step calculations and computer techniques using SPSS for Windows*, Psychology Press, 1998.

[32] Razali, N. M., Wah, Y. B., et al., "Power comparisons of shapiro-wilk, kolmogorov-smirnov, lilliefors and anderson-darling tests," *Journal of statistical modeling and analytics*, Vol. 2, No. 1, 2011, pp. 21–33.

[33] Shapiro, S. S. and Wilk, M. B., "An analysis of variance test for normality (complete samples)," *Biometrika*, Vol. 52, No. 3-4, 1965, pp. 591–611.

[34] Bland, J. M. and Altman, D. G., "Statistics notes: Cronbach's alpha," *Bmj*, Vol. 314, No. 7080, 1997, pp. 572.

[35] Cronbach, L. J., "Coefficient alpha and the internal structure of tests," *psychometrika*, Vol. 16, No. 3, 1951, pp. 297–334.

[36] Young, E. D., Fernandez, C., and Goldberg, J., "Responses of squirrel monkey vestibular neurons to audio-frequency sound and head vibration," *Acta oto-laryngologica*, Vol. 84, No. 1-6, 1977, pp. 352–360.

[37] Valente Pais, A. R., Van Paassen, M., Mulder, M., and Wentick, M., "Perception coherence zones in flight simulation," *Journal of Aircraft*, Vol. 47, No. 6, 2010, pp. 2039–2048.

Appendix A. Errors in Reporting

Appendix B. Tabular overview of the experiment results and overview of perception errors

A. Tabular overview

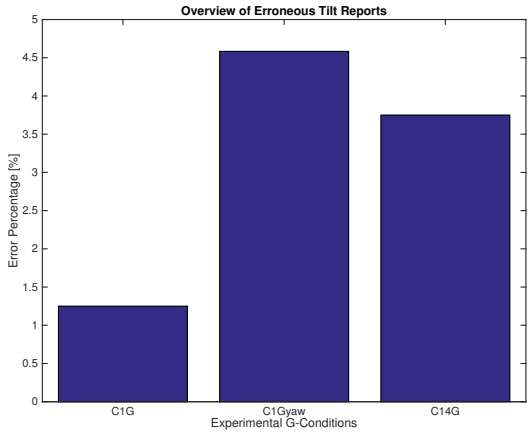

(a) Total percentage of incorrect tilt reports (perception errors) for 3 G-Conditions (1G,14G,1Gyaw).

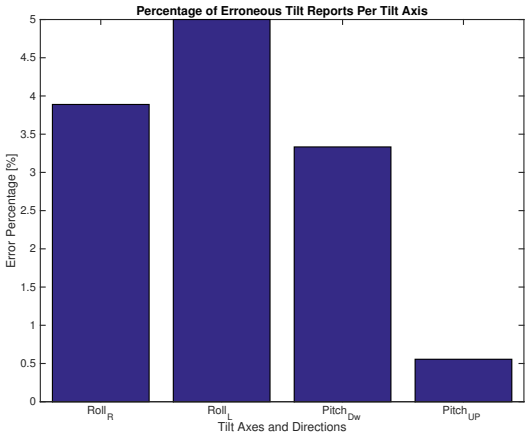

(b) Total percentage of incorrect tilt reports (perception errors) per Axis and Direction.

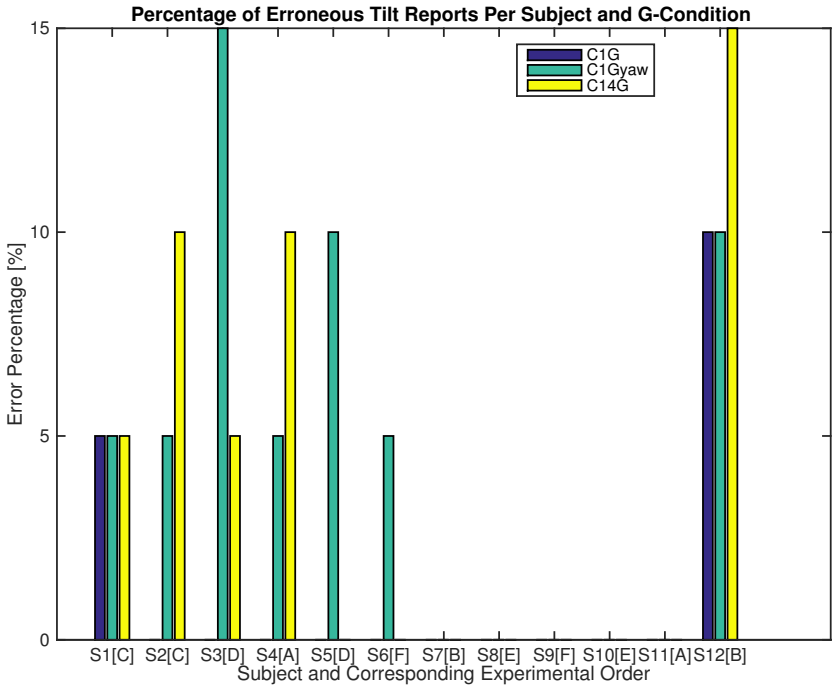

(c) Percentage of incorrect tilt reports (perception errors) per Subject and G-Condition. Latin letter A-F indicates starting order.

Figure 21 Overview of incorrect tilt reports (perception errors) for Axis, Direction and G-condition.

Table 4 Perceived mean threshold and standard deviation per G-Condition and Tilt. The values are shown for both excluding as including error reports. Values that show difference in both sets are printed in bold.

	Including Errors						Excluding Errors					
Measure	*mean*			*std*			*mean*			*std*		
Tilt/G-Condition	C1	C2	C3	C1	C2	C3	C1	C2	C3	C1	C2	C3
Roll Right	**4.068**	**5.638**	**3.945**	**1.686**	**2.625**	**1.859**	4.066	5.714	4.068	1.701	2.649	1.819
Roll Left	**4.140**	**5.647**	**4.182**	**1.478**	**2.350**	**1.998**	4.110	5.848	4.223	1.472	2.261	1.971
Pitch Down	6.512	**6.098**	**4.498**	3.691	**2.637**	**2.027**	6.512	5.993	4.467	3.691	2.661	1.981
Pitch UP	**5.657**	6.089	5.063	**2.488**	2.760	1.830	5.707	6.089	5.063	2.479	2.760	1.830

Table 5 Perceived median thresholds and Inter Quantile Range per G-Condition and Tilt. The values are shown for both excluding as including error reports. values that show difference in both sets are printed in bold.

	Including Errors						Excluding Errors					
Measure	*median*			*IQR*			*median*			*IQR*		
Tilt/G-Condition	C1	C2	C3	C1	C2	C3	C1	C2	C3	C1	C2	C3
Roll Right	**4.090**	**4.873**	**3.966**	**2.152**	**3.087**	2.680	4.078	4.922	3.990	2.171	3.024	2.611
Roll Left	**3.872**	**5.573**	**3.769**	**2.047**	**2.721**	2.602	3.863	5.648	3.816	2.031	2.720	2.602
Pitch Down	6.182	**5.458**	4.408	4.400	**4.248**	3.069	6.182	5.431	4.408	4.400	4.305	2.969
Pitch UP	**5.803**	6.281	5.178	**3.369**	4.117	2.788	5.901	6.281	5.178	3.309	4.117	2.788

Table 6 Adjacent values (min and max) corresponding to the threshold observations, per G-Condition and Tilt. The values are shown for both excluding as including error reports. Values that show difference in both sets are printed in bold.

	Including Errors						Excluding Errors					
G-Condition	C1		C2		C3		C1		C2		C3	
Tilt/Sign	min	max	min	max	min	max	min	max	min	max	min	max
Roll Right	1.214	7.461	1.389	10.279	**0.727**	8.572	1.214	7.461	1.389	10.279	1.014	8.572
Roll Left	1.549	7.795	1.538	10.090	1.021	9.075	1.549	7.795	1.538	10.090	1.021	9.075
Pitch Down	1.336	14.533	1.492	12.163	1.100	**8.305**	1.336	14.533	1.492	12.163	1.100	8.255
Pitch UP	1.591	10.571	1.851	13.417	0.611	8.165	1.591	10.571	1.851	13.417	0.611	8.165

Table 7 Outliers corresponding to threshold observations per G-Condition.

G-condition[a]	C1				C2				C3			
No./Tilt[b]	RR	RL	PD	PU	RR	RL	PD	PU	RR	RL	PD	PU
	max											
1	9.592	-	16.442	12.696	14.708	11.535	-	-	-	10.280	11.047	-
2	-	-	15.828	-	13.337	-	-	-	-	-	-	-
3	-	-	15.859	-	-	-	-	-	-	-	-	-
	min											
1	-	-	-	-	-	-	-	-	-	-	-	-

[a] Labels C1,C2 and C2 refer to the three experimental trials 1G, 1Gyaw and 1.4G, respectively.
[b] Labels RR, RL, PD, PU indicate Axis*Direction combinations, Roll, Pitch; and Right or Down, Left or Right.

Appendix C. Statistical Analysis Method & Normality, Reliability and Spericity Tests

1. Repeated Measures ANOVA Design

For current study a three-way Repeated Measures ANOVA design was chosen consisting to study the main and interaction effects of within factors, Direction, Axis and G-Conditions (Direction*Axis*G-Condition). The data format used in for the SPSS input is given in table 8.

Table 8 Within factors table used in the repeated measures anova test.

Axis[a]	*Direction* [b]	*G-Condition*[c]	*Dependent Variable*
1	1	1	RS1C1
		2	RS1C2
		3	RS1C3
	2	1	RS2C1
		2	RS2C2
		3	RS2C3
2	1	1	PS1C1
		2	PS1C2
		3	PS1C3
	2	1	PS2C1
		2	PS2C2
		3	PS2C3

[a] Axis levels: 1 = Roll, 2 = Pitch
[b] Direction levels: 1 = + (RR or PU) , 2 = - (RL or PD)
[c] G-Condition levels: 1 = C1 (1G), 2 = C2 (1Gyaw), 3 = C3 (1.4G)

While analysisng the data, an alternative Repeated Measures ANOVA scheme was considered (Nth-Observation·Tilt·G-Condition), where averaging of the over N-observations would not have been required. However, current approach was deemed suitable as no additional post hoc test were required to investigate the interaction of direction and axis, and it was able to deal with missing data points that were found for one subject.

2. Assumptions Regarding the Method & Supporting Tests

In order to test if the chosen approach was appropriate for the given data set, several statistical reliability and normality test were carried out on the sample data. The particular test, discussed thoroughly in the section Appendix C.A Appendix C.A.5 were the following:

- Mauchly's Test of Sphericity in Section Appendix C.A.1.
- Skewness and Kurtosis Normality Test Section Appendix C.A.2.
- Sharipo-Wilk Test in section Appendix C.A.3.
- Visual Examination of the Scatter Histograms and Q-Q plots in Section Appendix C.A.4/
- Chronbach's Alpha Reliability Test in Section Appendix C.A.5.

No statistical analysis was performed to study the order effects A-F. The purpose of randomising the starting order was to eliminate the learning effects. The sample data met all of the above mentioned statistical tests, hence the Repeated Measures ANOVA method used in the analysis was justified.

A. Statistical Test of Normality, Reliability and Sphericity

1. Mauchly's Test of Sphericity

The sample data was examined and all was found to satisfy the sphericity condition. The Mauchly's Test of Sphericity, as shown in table 9 the p values for the respective variables are Mauchly's test of sphericity was not violated .

alpha values are above 0.05.

Table 9 Mauchly's test of sphericity.

Measure:

Within Subjects Effect	*Mauchly's W*	*Approx. Chi-Square*	*df*	*p value*	Epsilon[c]		
					Greenhouse-Geisser	*Huynh-Feldt*	*Lower-bound*
Axis	1.000	0.000	0	-	1.000	1.000	1.000
Direction	1.000	0.000	0	-	1.000	1.000	1.000
G-condition	0.701	3.546	2	0.170	0.770	0.871	0.500
Axis * Direction	1.000	0.000	0	-	1.000	1.000	1.000
Axis * G-condition	0.606	5.008	2	0.082	0.717	0.795	0.500
Direction * G-condition	0.661	4.137	2	0.126	0.747	0.838	0.500
Axis * Direction * G-condition	0.893	1.131	2	0.568	0.903	1.000	0.500

[a] Tests the null hypothesis that the error covariance matrix of the orthonormalized transformed dependent variables is proportional to an identity matrix.
[b] Design: Intercept Within Subjects Design: Axis + Direction + G-condition + Axis * Direction + Axis * G-condition + Direction * G-condition + Axis * Direction * G-condition
[c] May be used to adjust the degrees of freedom for the averaged tests of significance. Corrected tests are displayed in the Tests of Within-Subjects Effects table.

2. Skewness and Kurtosis

The skewness and Kurtosis tests are used to examine how much the data deviates from the standard bell shaped normal distribution [31, 32]. The test is passed when the Skewness and Kurtosis z-values lie in the interval $[-1.96, 1.96]$. The calculation is as follows:

This test was performed for all twelve categories of the independent variable (Axis*Direction*G-Condition) and the results are presented in table 10. As seen the skewness was found to be [0.568, 0.880, 0.483,-0.370, 0.610, 1.199, 0.574, 0.153, -0.202, -0.264, 0.134, -0.939] (SE=0.637), for [RS1C1, RS1C2, RS1C3, RS2C1, RS2C2, RS2C3, PS1C1, PS1C2, PS1C3, PS2C1, PS2C2, PS2C3], respectively, and respective kurtosis values are [-1.004, 0.770, -0.089, -1.315, -0.096, 1.988, 0.107, -1.407, -0.651, -1.666, -1.485, -0.247](SE=1.232). The resulting z-values are all within the interval $[-1.96, 1.96]$. This means that the sample data passes is characterized with skewness and kurtosis measures that approximately match a normal distribution.

Table 10 Descriptive test of Skewness and Kurtosis values of the three-way ANOVA Sample Data. Labels indicate within factors: Axis (R,P), Direction (S1,S2) and G-Condition (C1,C2,C3).

Measure	**Skewness**			**Kurtosis**		
Source	***Statistic***	***Std. Error (SE)***	***z-value***	***Statistic***	***Std. Error (SE)***	***z-value***
RS1C1	0.568	0.637	0.891	-1.004	1.232	-0.815
RS1C2	0.880	0.637	1.381	0.770	1.232	0.625
RS1C3	0.483	0.637	0.758	-0.089	1.232	-0.072
RS2C1	-0.370	0.637	-0.581	-1.315	1.232	-1.067
RS2C2	0.610	0.637	0.958	-0.096	1.232	-0.078
RS2C3	1.199	0.637	1.881	1.988	1.232	1.614
PS1C1	0.574	0.637	0.900	0.107	1.232	0.087
PS1C2	0.153	0.637	0.240	-1.407	1.232	-1.142
PS1C3	-0.202	0.637	-0.317	-0.651	1.232	-0.528
PS2C1	-0.264	0.637	-0.415	-1.666	1.232	-1.352
PS2C2	0.134	0.637	0.210	-1.485	1.232	-1.205
PS2C3	-0.939	0.637	-1.474	-0.247	1.232	-0.200

3. Sharipo-Wilk

The null hypothesis for this test assumes that the data is normally distributed [32, 33]. The null hypothesis is rejected if p<0.005. The results presented in table 11 show that all p values for each category of the independent variables is above $\alpha = 0.05$ (p>0.05) hence the null hypothesis is accepted and the data can be assumed normally distributed according to Sharipo-Wilk test.

4. Visual Examination: Scatter Histograms and Q-Q plots

As a final normality test, a visual examination of the measured data was performed. The scattered normalized distributions showed that the sample data was consistent with approximate, expected normal distribution as shown in 14.

As a final normality test, a visual examination of the measured data was performed. The normal Q-Q plots, generated by SPSS, showed that the sample data was consistent with approximate normal distribution curve. Additionally, the data was examined by means of univariate histogram and scattered data plot, both per subject as per group data sorted by experimental trials. The scatter histograms, combination of scatter plots and marginal histograms, figures figs. 14b, 14d and 14f. Illustrate that the subject data approximately follows a normal bell shaped curve and that the majority of the data points are scattered in the neighborhood of the mean threshold. The curves are plotted for the respective within factors, direction (Right,Left) and (Down,UP), Axis (Roll,Pitch) G-Condition and with the exclusion of the outliers.

The definition of the outliers was discussed in section V.

To conclude, the normality tests suggest that the dependent variable, the perceived tilt, is approximately normally distributed for each category of independent variable. This justifies the use of parametric tests such as the repeated measures ANOVA, which is to be discussed in the following section.

Table 11 Results of Sharipo-Wilk and Kolmogorov-Smirnov test of normality on three-way ANOVA Sample Data. Labels indicate within factors: Axis (R,P), Direction (S1,S2) and G-Condition (C1,C2,C3).

Measure	**Kolmogorov-Smirnov**[b]			**Shapiro-Wilk**		
Source	***Statistic***	***df***	***p value***	***Statistic***	***df***	***p value***
RS1C1	0.164	12	0.200[a]	0.916	12	0.253
RS1C2	0.152	12	0.200[a]	0.945	12	0.569
RS1C3	0.182	12	0.200[a]	0.961	12	0.797
RS2C1	0.202	12	0.19	0.898	12	0.149
RS2C2	0.134	12	0.200[a]	0.945	12	0.570
RS2C3	0.147	12	0.200[a]	0.909	12	0.209
PS1C1	0.112	12	0.200[a]	0.962	12	0.815
PS1C2	0.142	12	0.200[a]	0.941	12	0.515
PS1C3	0.158	12	0.200[a]	0.923	12	0.310
PS2C1	0.156	12	0.200[a]	0.896	12	0.139
PS2C2	0.207	12	0.17	0.895	12	0.138
PS2C3	0.249	12	0.04	0.888	12	0.111

[a] *.Indicates lower bound of the true significance.
[b] Lilliefors Significance Correction.

5. Cronbach's Alpha Reliability Test

Aside from the normality test discussed in the previous section. The sample data was examined using the SPSS Cronbach's Alpha Test. This is a widely used method to test the reliability of psychometric experiments first described by Lee Chronbach in 1951 [34]. Lee proposed a method to asses if a set of test are measuring the same construct. Herein, he defined the expected correlation of these sets of test pertaining to a certain construct as the measure α [35].

The measure α, ranging from 0-1, is deemed acceptable when the value is above 0.7. The closer to one the better the internal consistency of the data. In our example the test is intended to asses if the thresholds measured belong to the same construct, the perceptual tilt thresholds observed by experimental subjects. This method can be used to test both

the three-way Repeated Measures ANOVA variables as the two-way variables, namely the threshold data per combined Axis*G-Condition. Conducting this test on the combined two factor data may is usefully in view of the underlying purpose of the established tilt thresholds as discussed earlier. Namely, combing these threshold values into buffering solution for alignment in either roll or pitch.

The results of the Cronbach's Alpha Test are summarized in table 12.

In case of three-way ANOVA, the measure α for total number of 12 variables is found to be 0.960, indicating excellent reliability (>> 0.70). Tle also shows the individual alpha values and if the alpha value can be improved in case the variable is removed from the data sets. As shown, all avalues are above 0.70.

Table 12 Results of Cronbach's Alpha reliability test on the three-way ANOVA Sample Data. Labels indicate within factors: Axis (R,P), Direction (S1,S2) and G-Condition (C1,C2,C3).

Measure	*Scale Mean if Item Deleted*	*Scale Variance if Item Deleted*	*Corrected Item-Total Correlation*	*Cronbach's Alpha if Item Deleted*
Source				
	57.531	382.857	0.832	0.958
RS1C2	55.960	343.651	0.882	0.954
RS1C3	57.654	372.613	0.805	0.957
RS2C1	57.459	389.645	0.810	0.959
RS2C2	55.952	352.547	0.892	0.954
RS2C3	57.416	369.957	0.818	0.956
PS1C1	55.087	316.476	0.812	0.962
PS1C2	55.439	344.176	0.875	0.954
PS1C3	57.101	364.528	0.880	0.955
PS2C1	55.942	359.784	0.772	0.957
PS2C2	55.509	343.990	0.843	0.955
PS2C3	56.536	372.026	0.848	0.956
	Total			
	Cronbach's Alpha	*Cronbach's Alpha Based on Standardized Items*	*N of Items*	
	0.960	0.970	12	

Appendix D. Detection Time of Angular and Linear Acceleration Cues

This section gives a brief overview perception limits of angular and linear acceleration cues in relation to detection time. The findings are intended to support the methodology and the assumption made for the experiment in section IV.

1. T_{detect} of Angular Acceleration Cues

Classical models of human sensory threshold include torsion pendulum models used to model the time decaying response of the SCC. Whereas these models are know to reasonably accurately model simple acceleration step responses they do not take into consideration the velocity requirement imposed on the capabilities of the SCC sensor[27]. As described by Guedry [6] and later by Young [27] the vestibular acceleration sensory threshold does not just depend on the magnitude of the acceleration but also on the magnitude of the velocity.

This critical velocity, also referred to as the Mulder product is the minimum detectable angular velocity for brief steps of acceleration. It is calculated as follows:

$$\omega_{min} = a_{min}\tau_L \tag{7}$$

Where a_{min} and τ_L , are, the minimum threshold acceleration ,the time constant of decay, respectively. The minimum threshold acceleration in the classical examples is the value, below which, the time to detect sharply approaches the infinity. These classical examples use the torsion-pendulum model to characterize the non-adapting semi circular canal response. The rising and decaying step response of the torsion-pendulum model is characterized by the time constant τ_L, estimated to lie in the region of 10-15s [27]. Figure 22a shows the relationship of time to detect, t_{detect} versus acceleration step input. Taking for 10s for τ_L, the assumed value for a_{min} becomes 0.25 $^\circ/s^2$. Using the equation above, these yield a value of, $\omega_{min} \approx 2.5\ ^\circ/s^2$. As shown, the time to detect becomes nearly infinite above values of approximately 0.5 rad/s^2.

The Mulder product, although expressing threshold limits in terms of velocity, is quite relevant for the preliminary experiment discussed in chapter IV. The cabin rotations used to introduce subject to tilt angle from upright position, are carried out at a constant angular velocity. It is relevant to establish that the constant rotational velocity lies below the Mulder product, ensuring that the accelerations during the short transient phase are not perceived by the SCC's.

2. T_{detect} of Linear Acceleration Cues

Likewise the estimation of linear acceleration cues is expected to have a time dependency. The time to detect. t_{detect} of the linear acceleration cues, is described by the latency of to detection steps of GIA relative to the subjects' upright (the orthogonal plane to estimated earth-centric horizontal). The perception of the linear acceleration cues, thus has a certain resolution as with intermediate acceleration steps. Figure 22b shows the decaying detection latency versus the steps of vertical linear acceleration from the subjects upright. The curve, a regression hyperbola fit of 8 subject data, yield a velocity constant of 0.022 $[G - units/s]$ and a minimum response time of 0.37 s.

Appendix E. Hosman's & van der Vaart's Generic SCC model

Models of the SCC have been an area of interest for man decades. One of the early studies by Fernandez and Goldberg [36] described a second-order filter model based on measurements of the neuronal activity of squirrel monkeys. Hosman and van der Vaart believed that the human vestibular response could be similarly modeled by means of second-order filter model. In their quest, they conducted a psychometric study to measure the perception thresholds of inertial motion. The transfer function found by Hosman et al., as given below, relates the input angular acceleration, $\ddot{\gamma}^\dagger$, to the output neuronal discharge rate, n_{SCC} [14]. In the presence of angular acceleration input, to output of the SCC is believed to yield in pure gain filtered perceptual angular acceleration $R_{\ddot{\gamma}}$ [37].

$$H_{SCC}(j\omega) = \frac{n_{SCC}}{R_{\ddot{\gamma}}} = \frac{(1 + 0.11j\omega)}{(1 + 5.9j\omega)(1 + 0.005j\omega)} \tag{8}$$

The transfer function could also be related mathematically, to input velocity, $\dot{\gamma}$. Adding a differentiator element, the transfer function, relating the velocity input to perceived velocity output can be rewritten to:

$$H_{SCC}(j\omega) = \frac{n_{SCC}}{R_{\dot{\gamma}}} = j\omega\frac{(1 + 0.11j\omega)}{(1 + 5.9j\omega)(1 + 0.005j\omega)} = j\omega H_{SCC}(j\omega) \tag{9}$$

†The notation γ refers to an angular displacement. Subsequently, $\dot{\gamma}$ and $\ddot{\gamma}$ denote the respective derivatives, the angular velocity and acceleration.

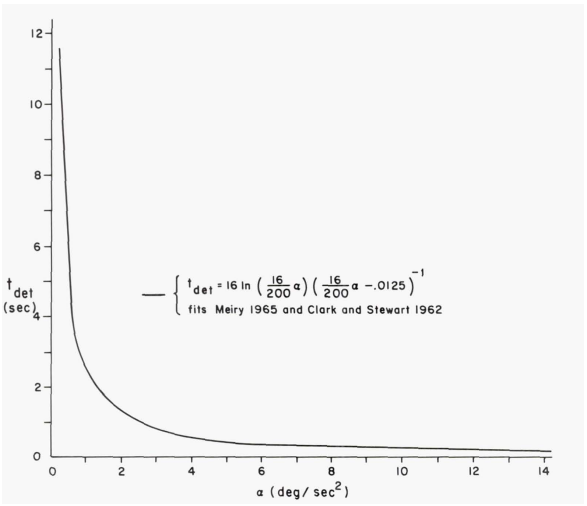

(a) Time to detect of a time step of yaw angular acceleration [27].

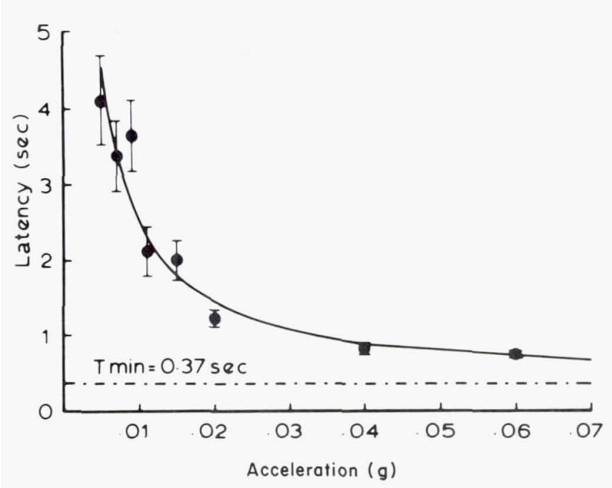

(b) Latency to detection of steps of vertical linear acceleration from the subjects upright. The model is taken from [27].

Figure 22 Detection time characteristics of angular and linear acceleration.

The thresholds they obtained were were 'pure', significantly smaller that most of the values know at the time. However they themselves, attributed this to 'good motion quality of the moving base flight simulator'. Additionally the focus on the task may very well influence the perception. In other words the actual thresholds, may not be as low, when the human is involved in simultaneous task.

Below a plot is shown of the responses of the Hosman et al. suggested SCC transfer function. As seen the rightmost plot, the human canal dynamics describe a nearly pure gain in the region of $\approx 0.5 - 5$ rad/s. We see that in this frequency the amplitude is nearly constant and phase is almost in sync. The acceleration diagram on the other hand closely resembles an integrator response.

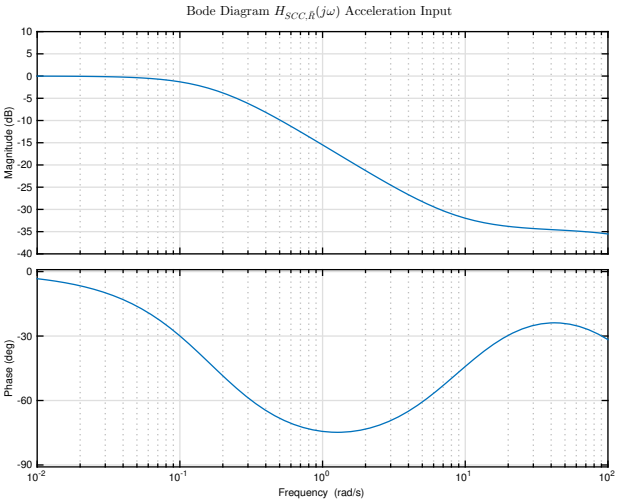

(a) Bode diagram of the SCC model with acceleration input.

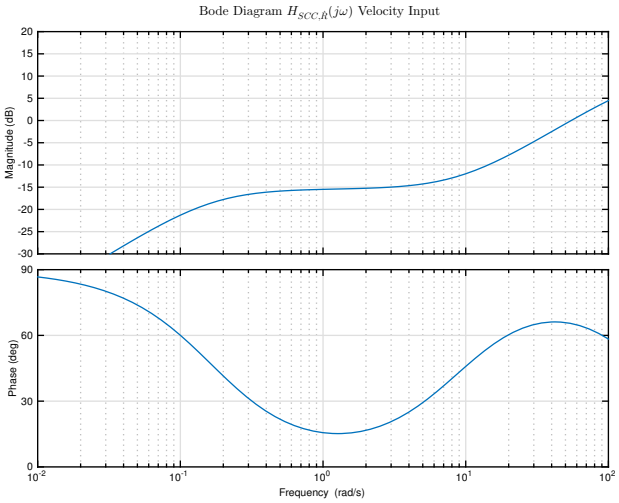

(b) Bode diagram of the SCC model with velocity input.

Figure 23 Bode diagrams of the SCC model described by Hosman et al. [14]